WILEY | ◉ Hindawi

Research Article

Development of Open Transport of Aqueous Fluid from Pegmatite Revealed by Trace Elements in Garnet

Astin Nurdiana ⓘ**, Atsushi Okamoto** ⓘ**, Masaoki Uno** ⓘ**, and Noriyoshi Tsuchiya** ⓘ

Graduate School of Environmental Studies, Tohoku University, Sendai 980-8579, Japan

Correspondence should be addressed to Astin Nurdiana; astin.nurdiana.d2@tohoku.ac.jp

We investigated the fluid flow and elemental transport from a granitic body to the middle crust by determining the trace element compositions of garnet in pegmatites related to a quartz diorite intrusion and metamorphic rocks on Kinkasan Island, northeast Japan. Garnet in the pegmatites and biotite schists is characterized by spessartine– (Sps–) almandine- (Alm-) rich compositions of $Sps_{14-69}Alm_{22-70}Prp_{2-14}Grs_{1-13}$ and $Sps_{16-30}Alm_{54-66}Prp_{9-16}Grs_{3-6}$, respectively. A garnetite pod in the metamorphic unit has grossular- (Grs-) rich compositions ($Sps_{1-4}Alm_{8-11}Prp_{0.1-0.4}Grs_{80-87}Adr_{3-4}$). The peak temperature (T) and pressure (P) conditions of the biotite schist during contact metamorphism were 600–650°C and 0.27–0.41 GPa, respectively. The primary fluid inclusions in quartz crystals within the pegmatites hosted by the quartz diorite and hosted by the metamorphic rocks have a wide range of homogenization temperatures (200–380°C). These correspond to the trapping temperature of 500–700°C, assuming a salinity of 4 wt.% $NaCl_{equivalent}$ at pressure of the crystallization of the quartz diorite. Chondrite-normalized rare earth element (REE) patterns of garnets in the pegmatites in the quartz diorite and metamorphic unit are generally characterized by enrichment of heavy REEs and negative Eu anomalies with the REE contents in the schists which are systematically lower than in the pegmatites. However, garnet in the biotite schists close to the pegmatites has similar REE contents to garnet in the adjacent pegmatites. These geochemical features suggest that garnet in the biotite schists grew in response to fluid infiltration from the pegmatites. Besides, the Grs-rich garnet in the garnetite pod and its host quartz schist have flat heavy REE patterns and no Eu anomalies, which probably reflect a metasomatic process related to plagioclase replacement that produced Ca-Al-rich fluids. Our results suggest that the infiltration of pegmatitic fluids enhances elemental transport and metamorphic reactions in the middle crust.

1. Introduction

Intrusion and solidification of hydrous magma is thought to be one of the most effective mechanisms for introducing aqueous fluids into the middle to upper crust of volcanic regions [1–3]. The emplacement and solidification of granitic bodies in the middle crust contributes to the formation of hydrothermal ore deposits [4, 5] and geothermal reservoirs with supercritical conditions [6, 7]. The late stages of solidification of hydrous magma often produce pegmatites, which record elemental as well as heat transfer [8–11]. However, the extent of element transfer from granitic pegmatites into adjacent crustal rocks is still poorly constrained. It is also unclear whether pegmatitic fluids affect contact metamorphism and vice versa.

Garnet is a common mineral in metamorphic rocks, and its growth zoning has been used to constrain pressure–temperature paths during regional metamorphism [12–15] and temperature–time paths during cooling and heating during contact metamorphism [16, 17]. The major and trace element contents of garnet can also provide information on fluid chemistry during metamorphism [18–20]. In the middle crust near plutons, garnet typically occurs not only in metamorphic rocks that formed during contact metamorphism but also in granitic pegmatites [21, 22]. Therefore, a comparison of garnet compositions in pegmatitic and

metamorphic rocks might provide key information regarding fluid compositions and elemental transport from plutonic rocks into the crust. However, there have been no previous studies that have directly compared the major and trace element compositions of garnet in pegmatites and surrounding metamorphic rocks.

Kinkasan Island in northeast Japan consists mainly of granodiorite and quartz diorite, abundant pegmatite dikes, and a minor metamorphic unit in contact with the plutons [23]. In a previous study [24], we showed that intensive feldspar replacement was induced by the sequential infiltration of Na- and K-rich fluids from the pegmatites into the metamorphic rocks under subsolidus conditions and that nano- to microscale porosity was generated within the altered feldspar grains. However, the trace element compositions of the pegmatitic fluids and processes of fluid migration into the metamorphic rocks are poorly constrained.

In this study, we investigated the compositional zoning and trace element chemistry of coeval garnets in pegmatites and surrounding metamorphic rocks on Kinkasan Island. Based on conventional geothermometry and a fluid inclusion study, we constrained the $P–T$ conditions of fluid infiltration and garnet growth in the pegmatites and metamorphic rocks. We then compared the trace element compositions of garnets in the pegmatites and metamorphic rocks, and we discuss the fluid transport and/or element fractionation during cooling of the midcrustal pluton.

2. Geological Setting and Samples

Kinkasan Island is 3.5×6.0 km in size and is located on the eastern coast of northeast Japan. The island is part of the South Kitakami Belt [25–27], which comprises granitoid and metamorphic basement rocks of Cambrian–Ordovician age and epicontinental sedimentary rocks of Silurian to Early Cretaceous age [28–30]. These sedimentary rocks in the South Kitakami Belt were strongly folded, faulted, and weakly metamorphosed during the Early Cretaceous Oshima Orogeny [31] and then intruded by granitic magma during the Early Cretaceous [25]. Kinkasan Island consists mainly of Early Cretaceous quartz diorite and granodiorite (Figure 1(a)) and a metamorphic unit that crops out along the northwestern coast at a contact with the quartz diorite (Figure 1(b)). The metamorphic unit is largely below sea level but is exposed as narrow outcrops. The metamorphic unit is not continuous across to Oshika Peninsula, which is located on the opposite side of Kinkasan Island [32]. Zircon U–Pb ages of the intrusions on Kinkasan Island are 121 ± 2 Ma for the central biotite–hornblende tonalite, 122 ± 2 Ma for the marginal granodiorite, and 128 ± 2 Ma for the biotite–hornblende tonalite dike [33]. Biotite K–Ar ages of the granitoids are 122 and 112 Ma for the western and eastern parts of Kinkasan Island [34], respectively, but there are no age data for the metamorphic unit. However, in the Hitachi metamorphic unit as a part of South Kitakami Belt [25], the age of metamorphism was determined based on mica K–Ar dating which yielded 120–105 Ma and occurred due to granite emplacement [35].

Along the northwestern coast of Kinkasan Island, schistose hornblende–biotite-bearing quartz diorite (Qz diorite) is exposed in the northern and southern parts of the metamorphic unit (Figure 1(b)). The quartz diorite contains a weak foliation that is defined by the alignment of hornblende [24] with a common strike of N10°–20°E and dips 50°–80° to the west, which is largely concordant with the foliation of the metamorphic rocks [23, 32]. Based on hornblende–plagioclase geothermometry and Al-in-hornblende geobarometry, the $P–T$ conditions of crystallization of the plutonic body were estimated to be 670–760°C and 0.30–0.45 GPa [24, 32]. The quartz diorite is cut by abundant pegmatite dikes with widths of 5–40 cm, which dominantly strike NE–SW. The thick pegmatites (>10 cm width) consist mainly of quartz, plagioclase, K-feldspar, and biotite, along with accessory garnet, ilmenite, magnetite, and zircon. These pegmatites hosted by the Qz diorite have sharp boundaries with their host rocks and are typically cut by thin (~1 cm width) aplite veins.

The metamorphic unit consists mainly of biotite (Bt) schist with intercalations of clinopyroxene (Cpx) schist, amphibole (Amp) schist, quartz schist, and garnet schists [23, 24, 30, 36]. The foliation in the schists strikes NE–SW and dips 70°–90° to the west. By applying garnet-biotite thermometry and garnet-plagioclase-sillimanite-quartz geobarometry, Endo et al. [32] estimated the $P–T$ conditions of the biotite schists to be 580–650°C and 0.20–0.37 GPa. The crystallization pressure of the plutonic body is similar to or slightly higher than the pressure estimated from surrounding metamorphic rocks, suggesting that contact metamorphism occurred in response to the granitoid intrusion into the relatively shallow crust [32]. Pegmatites and aplites occur extensively in the metamorphic unit near the contact with the Qz diorite. Infiltration of pegmatitic fluids into the metamorphic rocks is occasionally marked by millimeter-scale reaction zones around the pegmatites and myrmekite [24]. Based on petrological analyses of the reaction zone within the Cpx schists using hornblende–plagioclase geothermometry, and analyses of the replacement of plagioclase in an amphibole schist by two-feldspar thermometry, Nurdiana et al. [24] showed that the pegmatitic fluids caused extensive metamorphism and hydrothermal alteration around the intrusion. The fluid compositions changed from Na-rich during the initial solidification stage at 640–730°C to K-rich during cooling of the plutonic body to 400–570°C [24].

2.1. Sample Descriptions. Major and trace element compositions of garnet were determined for seven garnet-bearing samples; three pegmatites, and four metamorphic rock samples. Total sample is seven which consist of three pegmatites and four metamorphic rock samples. The sampling localities are shown in Figure 1. The pegmatite samples include those hosted by Qz diorite (sample PgD; Figure 2(a)), Cpx schist (sample PgC; Figure 2(b)), and Bt schist (sample PgB; Figure 2(c)). The metamorphic rocks analyzed in this study are two Bt schists (samples BSa and BSb), a quartz schist (Qz schist; sample QS), and a garnetite pod adjacent to the quartz schist (sample POD; Figure 2(d)). The mineral assemblages of the samples are listed in Table 1. Some biotite
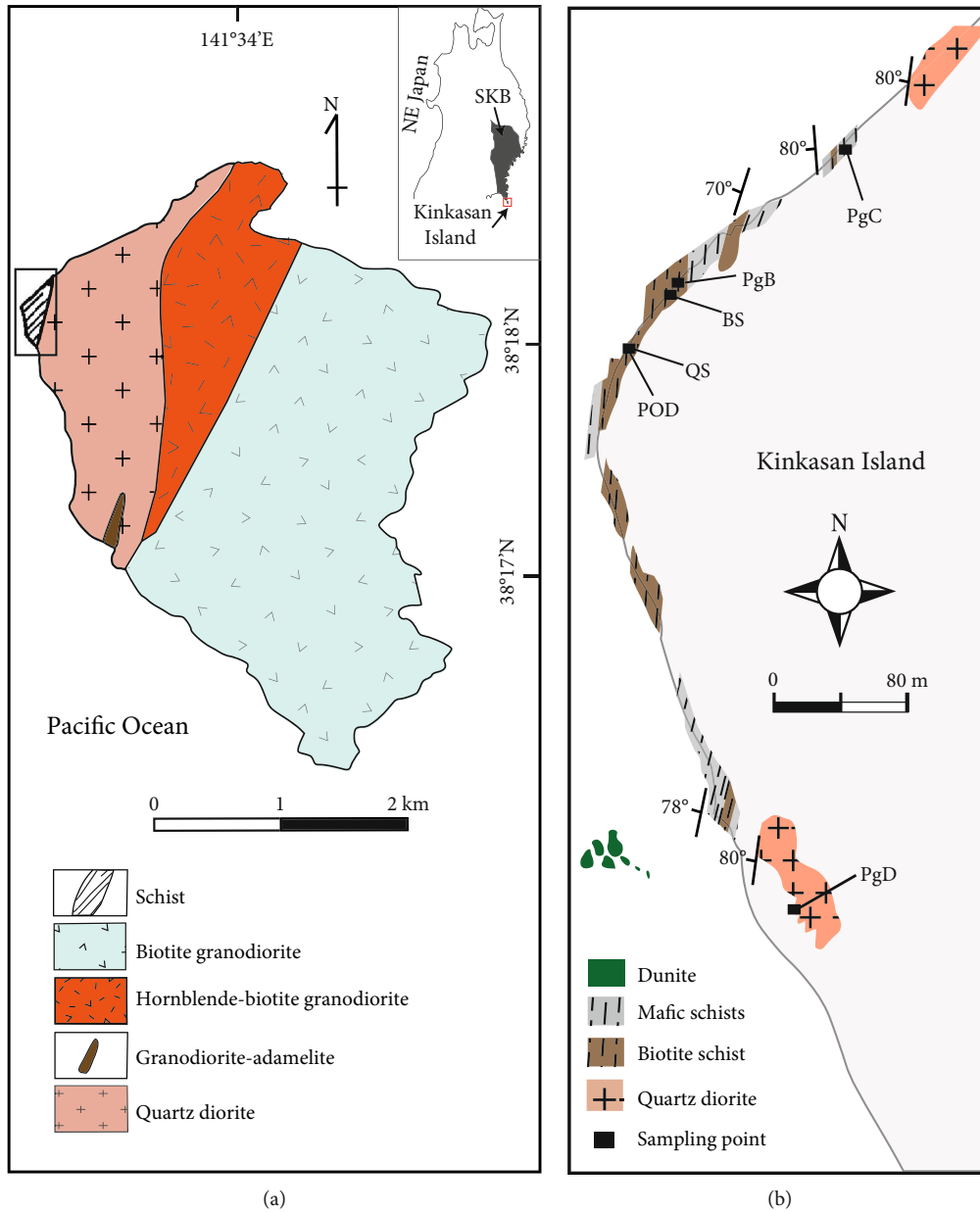
FIGURE 1: (a) Simplified geological map of Kinkasan Island (modified after Kobayashi [62]). The open rectangle indicates the study area. (b) Map of the metamorphic unit and quartz diorite along the northwestern coastline of Kinkasan Island (modified after Inoki et al. [23] and Nurdiana et al. [24]), showing the sampling locations. PgD: Qz diorite-hosted pegmatite; PgC: Cpx schist-hosted pegmatite; PgB: Bt schist-hosted pegmatite; BS: Bt schist; QS: Qz schist; POD: garnetite pod.

schist samples contain isolated garnet grains (~0.5 mm; 1 area%; sample BSa), and sample BSb contains abundant garnet of variable sizes (0.05–1 mm; 8 area%). The pegmatite veins hosted by the Bt schist (sample PgB) are parallel to the schistosity (Figure 2(c)). The garnetite pod is enclosed by quartz schist (Figure 2(d)).

3. Methods

Major and some trace elements (Y and Ti) were analyzed with an electron probe microanalyzer (EPMA; JEOL JXA-8200) at Tohoku University, Tohoku, Japan. The accelerat-ing voltage was 15 kV, and the beam current was 12 nA for quantitative analyses and 120 nA for elemental mapping. Trace element mapping of garnet was carried out with an accelerating voltage of 25 kV and beam current of 490 nA. The dwell time for the major and trace element mapping was 30 ms. The following minerals were used as major element standards: wollastonite (SiO_2 and CaO), corundum (Al_2O_3), hematite (FeO), periclase (MgO), manganosite (MnO), albite (Na_2O), K-feldspar (K_2O), and rutile (TiO_2). Hereafter, the compositions of garnet are denoted by the mole percent of spessartine (Sps), almandine (Alm)+pyrope (Prp), grossular (Grs), and andradite (Adr) in the format of
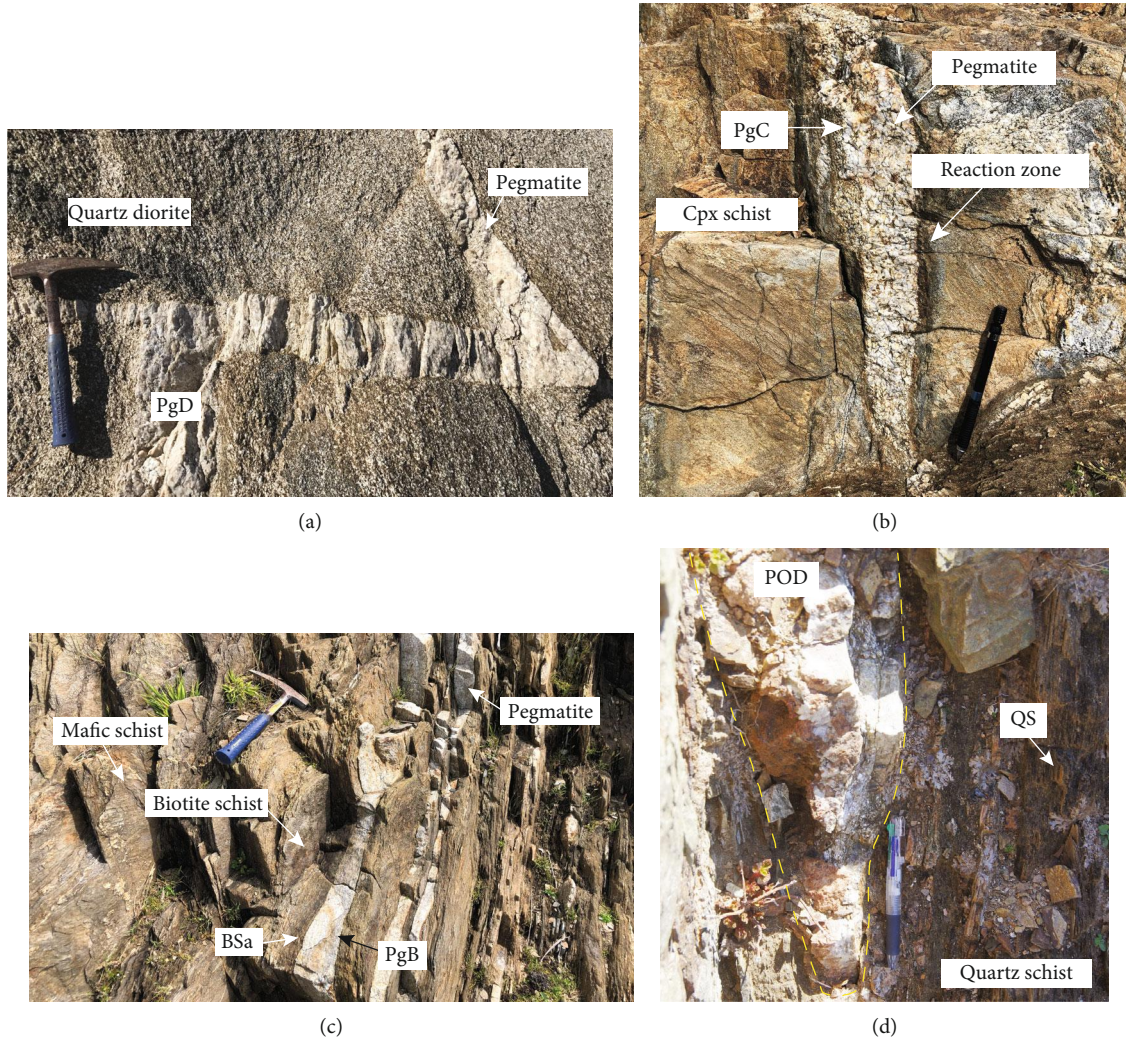
(a)

(b)

(c)

(d)

Figure 2: Outcrop photographs of (a) pegmatites in quartz diorite (PgD), (b) a pegmatite (PgC) intruded into mafic schist marked by a reaction zone at the pegmatite border, (c) pegmatites intruded subparallel to the foliation in schist, and (d) a garnetite pod (POD) in quartz schist (QS). PgD: Qz diorite-hosted pegmatite; PgC: Cpx schist-hosted pegmatite; PgB: Bt schist-hosted pegmatite; BS: Bt schist; QS: Qz schist; POD: garnetite pod.

Table 1: Mineral assemblages and modal abundances (area%) of all sample groups from Kinkasan Island.

No.	Sample	Mineral assemblage	Qz	Pl	Kfs	Bt	Grt	d_{garnet} (mm)	x_{garnet} (cm)	Minor minerals
Pegmatites										
1	PgD	Kfs-Qz-Pl-Bt	30	28	40	1		0.3–1	1–5	Mag-Zrn-Ilm
2	PgB	Kfs-Qz-Pl-Bt-Grt	20	15	53	8	2	1–1.2	0.25–1.5	Ms-Chl-Ser-Ap-Zrn-(Mnz-Ce)
3	PgC	Pl-Qz-Kfs-Grt	45	37	15		2	0.8–1.2	0.5–5	Mag
Biotite schists										
4	BSa	Pl-Qz-Bt-Grt	25	40		33	1	~0.5	~1	Ap-(Mnz-Ce)-Zrn
5	BSb	Qz-Bt-Pl-Grt	60	12		16	8	0.05–1	>100	Ms-Chl-Kln
Garnetite pod and adjacent quartz schist										
6	QS	Qz-Bt-Grt-Pl	85	1		7	7	0.1–0.3	>100	Ap
7	POD	Grt-Qz	1				98	20–30	>100	Mag

d: grain or pod size of garnet; *x*: the distance of garnet to the closest contact of pegmatite dike-schist. Abbreviations: Qz: quartz; Pl: plagioclase; Kfs: K-feldspar; Bt: biotite; Grt: garnet; Mag: magnetite; Ms: muscovite; Chl: chlorite; Ser: sericite; Kln: kaolinite; Zrn: zircon; Ilm: ilmenite; Ap: apatite; Mnz-Ce: monazite-Ce.

$Sps_{60}Alm+Prp_{33}Grs_5Adr_2$. The andradite component was only found in garnet from the sample POD. The end-member garnet components, including ferric iron, were calculated based on Locock [37]. The modal abundances of the minerals were taken to be the area percentage of each mineral and were determined based on analyses of the back-scattered electron (BSE) images using ImageJ software.

Trace element contents in garnet were determined by laser ablation–inductively coupled plasma–mass spectrometry (LA–ICP–MS) at Tohoku University, using a PerkinElmer ELAN ICP–MS system coupled to a Photon Machines/CETAC Analyte Excite 193 nm excimer LA system. Single-spot LA was conducted on all samples, which involved 120 laser shots at a pulse energy of 9.45 J/cm^2, with a laser repetition rate of 10 Hz and laser beam diameter of 50 μm. Helium was used as the carrier gas. ^{29}Si was used as the internal standard, and the NIST 612 glass was used as an external standard. The reference values of NIST 612 were taken from Jochum et al. [38]. A total of 40 trace elements were analyzed, and the data were screened for inclusions. Trace element data were normalized to the chondritic values of Taylor and McLennan [39].

Fluid inclusion microthermometry in quartz was conducted on doubly polished thick sections. The homogenization temperatures (T_h) and ice melting temperatures were determined with a heating–cooling stage (Linkam THMS 600) at Tohoku University. A synthetic quartz inclusion was used for calibration. The precision of the homogenization temperatures is ±1°C. The stage is observed with an Olympus DP74 microscope with 40x and 100x magnification. The homogenization temperatures were measured in quartz from pegmatite samples PgD, PgC, and PgB. The isochore calculation was based on the H_2O–NaCl isochore of Bodnar [40]. The density of saline fluid was calculated following the equation of state proposed by Zhang and Frantz [41] using BULK software [42].

4. Petrography and Mineral Compositions

Representative chemical compositions of plagioclase, biotite, and garnet are listed in Table 2. Figure 3 shows the mineralogy of representative samples. The chemical compositions of plagioclase and biotite are plotted in Figure 4. The cations in biotite were allocated to sites based on the method of Rieder et al. [43].

4.1. Pegmatites. The mineralogy of the pegmatites (and aplites) is variable which typically consists of elongated, coarse-grained plagioclase, quartz, K-feldspar, and minor biotite, garnet (Grt), magnetite (Mag), ilmenite (Ilm), zircon (Zrn), and monazite-(Ce) (Mnz-Ce; Figure 3(a)). In the pegmatite hosted by the quartz diorite (sample PgD), the modal abundance of plagioclase was 28 area%, quartz was 30 area%, and that of K-feldspar was 40 area%. Sample PgB has 15 area% plagioclase, 20 area% quartz, and 53 area% K-feldspar. Sample PgC has 37 area% plagioclase, 45 area% quartz, and 15 area% K-feldspar. The pegmatites have typical aplitic, graphic, and/or blocky textures, with grain sizes of 1–50 mm depending on pegmatite thickness. The anor-

thite (An) contents of plagioclase vary between the samples and are An_{9-16} in sample PgD, An_{27-55} in sample PgC, and An_{15-29} in sample PgB (Figure 4(a)). Plagioclase is generally zoned, with decreasing An contents from core to rim. Plagioclase grains in samples PgD and PgB have been partly replaced by albite with a composition of $An_{0-1}Ab_{99-100}$ [24]. Biotite in pegmatites has a wide range in compositions (Figure 4(b)), with X_{Mg} (Mg/[Mg + Fe^{tot}]) of 0.78–0.81 per formula unit (p.f.u.; O = 11 atoms), 0.51–0.62 p.f.u., and 0.58–0.60 p.f.u., respectively, for PgD, PgC, and PgB. Al occupancy in the tetrahedral site (Al [T]) is 0.63–0.78 p.f.u. for PgD, 1.31–1.56 p.f.u. for PgC, and 1.34–1.61 p.f.u. for PgB, while Ti is ~0.002 p.f.u., 0.22–0.13 p.f.u., and 0.002–0.20 p.f.u., respectively, for PgD, PgC, and PgB. Garnet occurs as subhedral or euhedral grains that are 0.3–1.2 mm in size (Figure 3(b)). The garnets are generally clustered in the center of the thick pegmatite dikes (Figure 3(a)). Some garnet contains inclusions of quartz. In sample PgB, garnet occurs in a biotite-rich layer with secondary chlorite (Chl) and sericite (Ser).

4.2. Biotite Schists. The biotite schists consist of quartz (25 area%–60 area%), plagioclase (12 area%–40 area%), biotite (16 area%–33 area%), and lesser K-feldspar, muscovite, chlorite, garnet, and apatite. Plagioclase compositions vary from An_{26-41} (Figure 4(a)), with increasing An contents from core to rim. Secondary plagioclase (albite) occurs along the plagioclase rims. Biotite has a rather homogeneous composition, with $X_{Mg} = 0.60 - 0.70$, Al [T] = 1.35 – 1.63 p.f.u., and Ti = 0.03 – 0.15 p.f.u. (Figure 4(b)). Garnet occurs as euhedral grains that are 0.05–1 mm (average = 0.5 mm) in size and is commonly found in biotite-rich layers. One sample of biotite schist (BSa), collected from the contact with a pegmatite, contains relatively large garnet grains that are ~0.5 mm in size (Figures 2(c), 5(e), and 6(d)), and garnet occurs preferentially in a zone that is >10 mm from the contact. The other sample of biotite schist (BSb) contains abundant garnet grains (0.05–1 mm) and was collected >1 m from a pegmatite (Figures 3(c) and 3(d)). Apatite is 0.05–0.2 mm in size and occurs uniformly in the Bt schists.

4.3. Garnetite Pod and Adjacent Quartz Schist. The Qz schist sample (QS) consists mainly of quartz (85 area%), biotite (7 area%), and garnet (7 area%) and lacks plagioclase. Biotite occurs as platy grains that are 0.1–0.3 mm in size and typically occurs on garnet rims. The biotite composition is $X_{Mg} = 0.54 - 0.58$, Al [T] = 0.91 – 1.43 p.f.u., and Ti = 0.05 – 0.13 p.f.u. (Figure 4(b)). Apatite inclusions are abundant in garnet cores. The garnetite pod (sample POD) is 20–30 cm long and surrounded by Qz schist (Figure 2(d)). The sample POD consists almost entirely of garnet (>98%) and minor quartz and magnetite (Figures 3(e) and 3(f)).

5. Major Element Compositions of Garnet

Representative major element compositions of garnet and other minerals are listed in Table 2 and shown in Figures 5 and 6.

TABLE 2: The representative composition of garnet, biotite, and plagioclase in Kinkasan Island.

	Garnet in pegmatites			Garnet in schists			Biotite		Plagioclase	
Host rock	Qz diorite[a]	Cpx schist[a]	Bt schist[a]	Bt schist	Qz schist	Garnetite pod	Pegmatite in Bt schist	Bt schist	Pegmatite in Bt schist	Bt schist
Sample	PgD	PgC	PgB	BS	QS	POD	PgB	BS	PgB	BS
SiO_2	36.26	36.6	37.44	37.49	37.6	39.44	35.61	35.4	62.2	61.51
TiO_2	0.56	0.22	0.03	b.d.l.	0.03	0.14	2.42	3.07	b.d.l.	0.05
Al_2O_3	19.15	20.73	21.63	22.11	21.19	21.57	19.27	19.82	23.72	24.51
FeO	10.27	20.28	30.35	28.49	27.38	5.89	19.95	17.72	0.04	0.03
MnO	29.75	19.99	7.63	6.77	8.06	0.75	0.45	0.32	b.d.l.	b.d.l.
MgO	0.92	0.54	2.97	3.68	1.72	0.05	7.93	9.94	0.04	0.02
CaO	2.46	1.69	0.29	1.4	4	32.35	0.07	b.d.l.	4.59	5.45
Na_2O	0.05	0.02	b.d.l.	0.03	0.01	b.d.l.	0.07	0.11	8.39	7.97
K_2O	b.d.l.[b]	b.d.l.	b.d.l.	b.d.l.	b.d.l.	b.d.l.	10.24	10.48	0.18	0.29
Total	99.42	100.07	100.35	99.97	99.99	100.2	96.01	96.86	99.34	99.84
	Cation per 12 oxygens						11 oxygens		8 oxygens	
Si^{4+}	3	2.99	3	2.99	3.02	3	2.71	2.65	2.77	2.73
Ti^{4+}	0.04	0.01	0	—	0	0.01	0.14	0.17	—	—
Al^{3+}	1.86	2	2.04	2.07	2.01	1.94	1.73	1.75	1.25	1.28
Fe^{2+}	0.6	1.39	2.03	1.9	1.84	0.32	1.27	1.11	—	—
Fe^{3+}[c]	0.12	0	0	0	0	0.06	—	—		
Mn^{2+}	2.08	1.38	0.52	0.46	0.55	0.05	0.03	0.02	—	—
Mg^{2+}	0.11	0.07	0.35	0.44	0.21	0.01	0.9	1.11	—	—
Ca^{2+}	0.22	0.15	0.02	0.12	0.34	2.64	0.01	—	0.22	0.26
Na^+	—	—	—	—	—	—	0.01	0.02	0.72	0.69
K^+	—	—	—	—	—	—	0.99	1	0.01	0.02
Total	8.03	7.99	7.98	7.98	7.97	8.02	7.79	7.83	4.97	4.98
X_{Prp}	0.04	0.02	0.12	0.14	0.07	0				
X_{Alm}	0.21	0.46	0.66	0.61	0.61	0.11				
X_{Sps}	0.73	0.46	0.17	0.15	0.18	0.02				
X_{Grs}	0	0.05	0.05	0.01	0.14	0.86				
X_{Adr}	0.02					0.01				
$X_{Al,Bt}$[d]							0.16	0.14		
An									22.96	26.95
Ab									75.97	71.35
Or									1.08	1.7
P (GPa)[e]			0.20–0.39	0.27–0.41						
T (°C)[e]			630–660	600–650						

[a]Pegmatite dike host rock. [b]b.d.l.: below detection limit. [c]Fe^{3+} of garnet was calculated on the basis of 12 oxygens following Locock [37]. [d]$X_{Al,Bt} = Al^{VI}/(Fe^{2+} + Mg + Al^{VI} + Ti)$. [e]P-T estimates based on GB-GBPQ [44, 45].

Garnet in the pegmatite samples (PgD, PgC, and PgB) is typically enriched in Sps (14–69 mol%) and Alm (22–70 mol%) and contains minor amounts of Prp (2–14 mol%) and Grs (1–13 mol%). Garnet in the quartz diorite-hosted pegmatites (sample PgD) has a Sps-rich composition ($Sps_{57–69}$) and subordinate Alm component ($Alm_{22–30}$), while garnet in the Cpx schist-hosted pegmatites (sample PgC) has moderate Sps (38–48 mol%) and Alm+Prp contents (48–58 mol%; $Alm_{44–54}$ and $Prp_{2–4}$) (Figure 5(a)). Garnet in samples PgD and PgC exhibits zoning characterized by decreasing Sps and increasing Alm and Grs contents

from core to rim (Figures 5(b) and 5(c) and Figures 6(a) and 6(b)). Garnet in the Bt schist-hosted pegmatites (sample PgB) is Alm+Prp-rich ($Alm_{65–70}$ and $Prp_{9–14}$), with a slight increase in Mn contents at the garnet rims. Prp contents exhibit an abrupt decrease at the rims, and the Grs contents are irregularly zoned (Figures 5(a) and 5(d) and Figure 6(c)).

Garnet in the Bt and Qz schists is mostly enriched in Alm+Prp and contains minor Sps. Garnet in the Bt schist (BS) has a dominant Alm+Prp composition (66–80; $Alm_{54–66}$ and $Prp_{9–16}$) but exhibits an abrupt increase in Mn and decrease in Mg–Fe contents at garnet rims
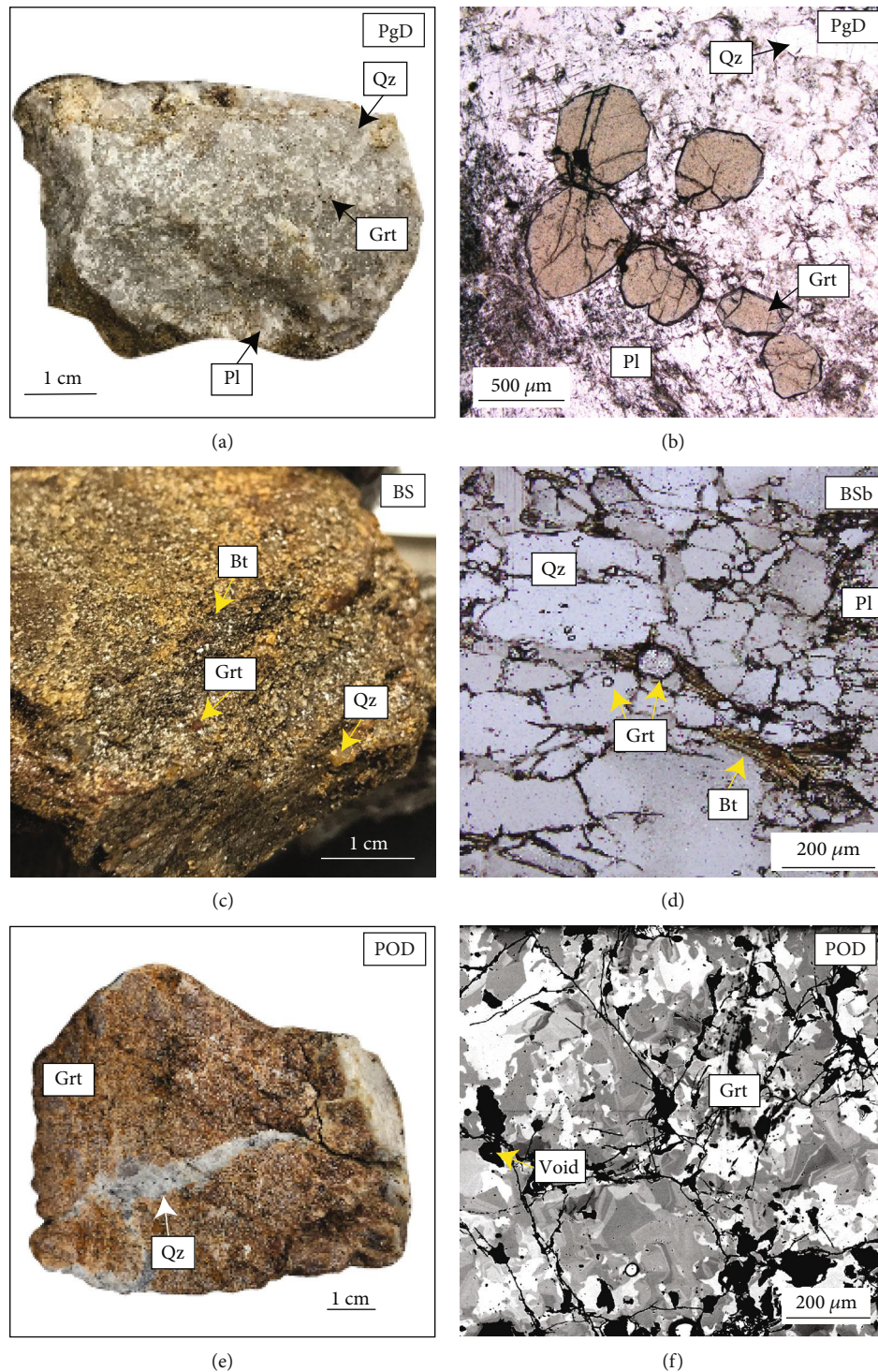
FIGURE 3: Hand specimen photographs and photomicrographs (plane-polarized light) of typical garnet in samples of (a, b) pegmatite (PgD) and (c, d) biotite schist (BS). (e) Hand specimen photograph of a garnetite pod (POD) and (f) back-scattered electron (BSE) image of irregular elemental zoning in a POD. White to dark gray shading indicates the intensity of the back-scattered electrons from high to low. Bt: biotite; Grt: garnet; Pl: plagioclase; Qz: quartz; PgD: Qz diorite-hosted pegmatite; PgC: Cpx schist-hosted pegmatite; PgB: Bt schist-hosted pegmatite; BS: Bt schist; QS: Qz schist; POD: garnetite pod.

(Figures 5(a) and 5(e) and Figure 6(d)). Garnet in the Qz schist (sample QS) has an Alm+Prp content of 69–73 mol% (Alm_{62-66} and Prp_{6-8}) with Grs_{9-13} (Figure 5(a)). The garnet in the Qz schist exhibits irregular zoning

of Grs, with high-Grs regions being close to apatite (Figures 5(f) and 6(e)).

In contrast to the Bt and Qz schists, the garnet in the garnetite pod has high Ca contents (Figure 5(a)). Garnet in
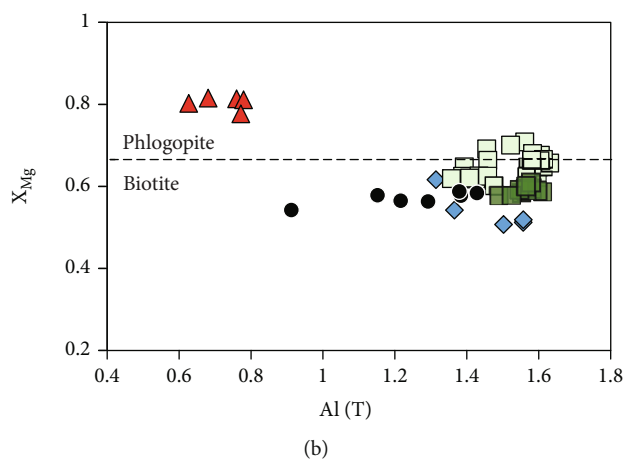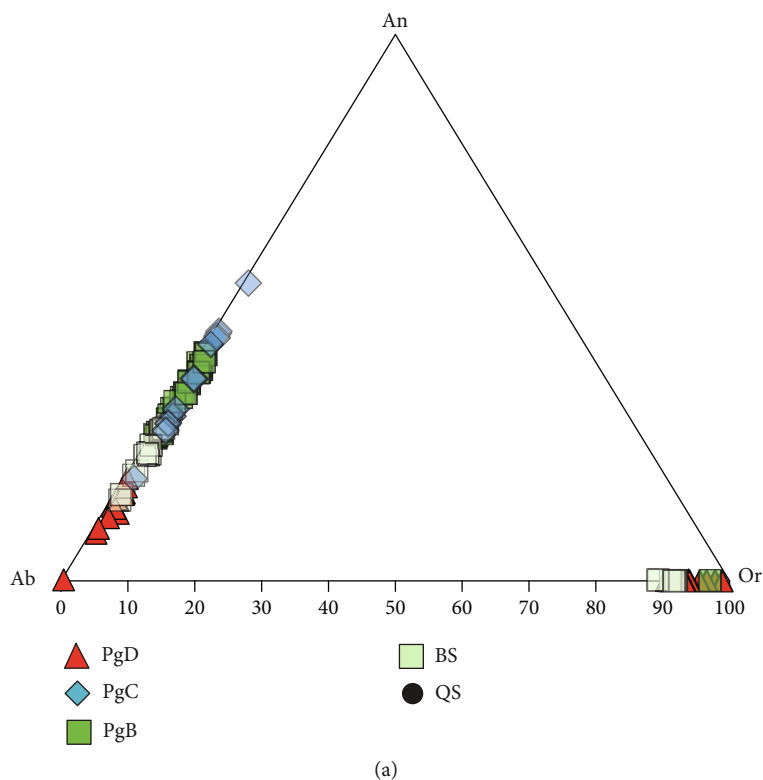
FIGURE 4: Compositions of plagioclase and biotite in the studied samples. (a) Ternary diagram of feldspar composition in pegmatite and biotite schist. (b) Al contents in the tetrahedral site and X_{Mg} values ($X_{Mg} = $ Mg/[Mg + Fe^{tot}]) of biotite in schist (per formula unit [p.f.u.]; O = 11 atoms). Ab: albite; An: anorthite; Or: orthoclase; PgD: Qz diorite-hosted pegmatite; PgC: Cpx schist-hosted pegmatite; PgB: Bt schist-hosted pegmatite; BS: Bt schist; QS: Qz schist; POD: garnetite pod.

the garnetite pod (sample POD) is primarily Grs (80–87 mol%), with negligible Prp (Figure 5(a)) and Adr (3–4 mol%), as revealed by the depletion of Al [T]. The garnet in the sample POD exhibits irregular zoning of Al, Ca, and Fe (Figures 3(f), 5(g), and 6(f)).

6. Trace Element Compositions of Garnet

Representative trace element (including rare earth element [REE]) data are shown in Figure 7 and listed in Table S1 (Supplementary Material). The terms light and heavy REEs refer to the elements La–Sm and Gd–Lu, respectively. The

chondrite-normalized REE patterns of garnet are shown in Figures 7(a)–7(f), and the multitrace element pattern is shown in Figure S1 (Supplementary Material). The variations of the REE patterns are evident from plots of Eu anomalies (Eu/Eu*) versus total REE contents (ΣREE) (Figure 7(g)), Sm versus Gd (Figure 7(h)), Y versus Σ REE (Figure 7(i)), and Y versus Ti (Figure 7(j)).

6.1. *Rare Earth Elements*. Garnets in the pegmatites (Figures 7(a)–7(c)) and Bt schist (Figure 7(d)) are depleted in light REEs and enriched in heavy REEs. In contrast, the garnets in the quartz schist (Figure 7(e)) and garnetite pod
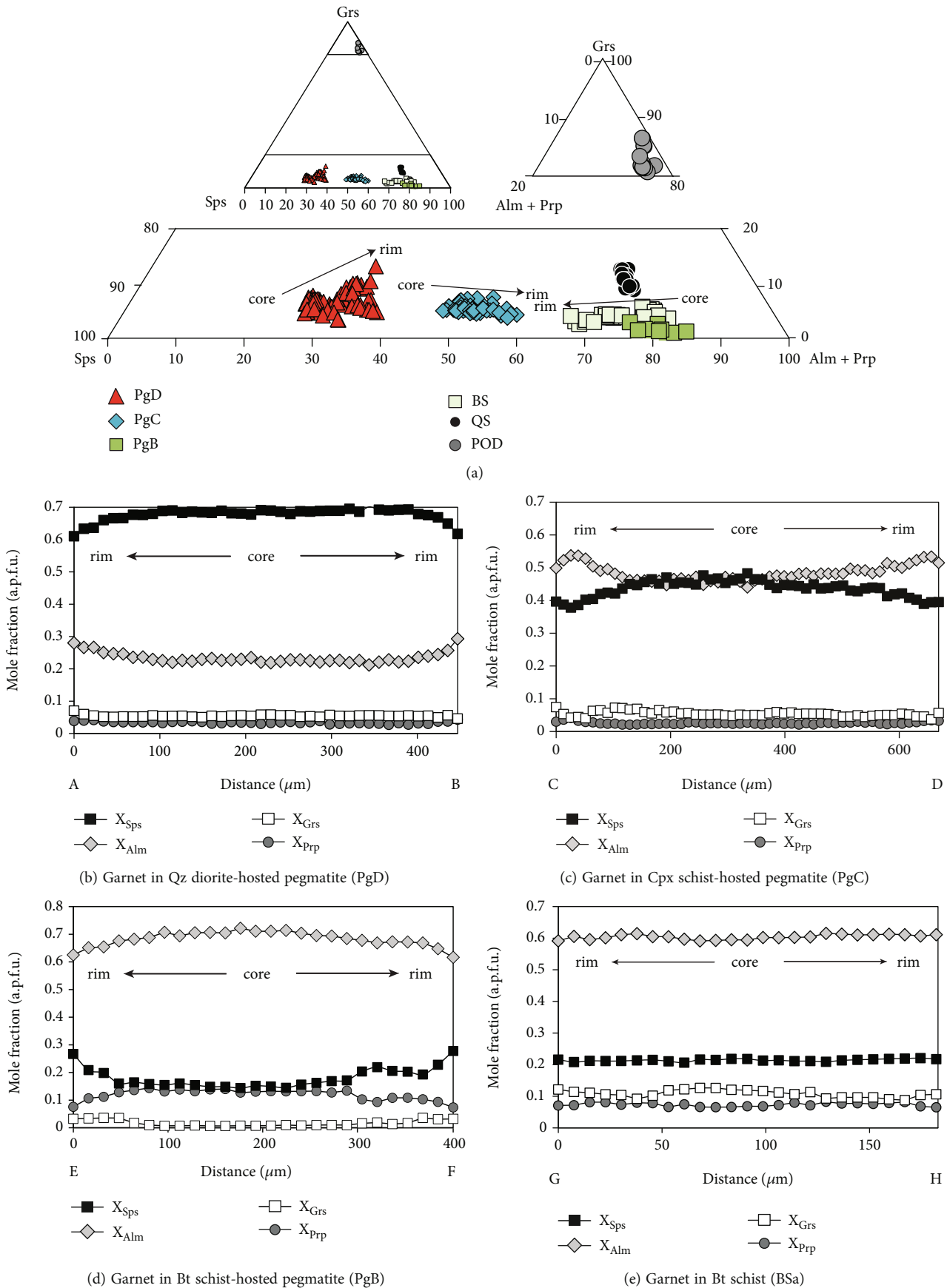
(a)

(b) Garnet in Qz diorite-hosted pegmatite (PgD)

(c) Garnet in Cpx schist-hosted pegmatite (PgC)

(d) Garnet in Bt schist-hosted pegmatite (PgB)

(e) Garnet in Bt schist (BSa)

FIGURE 5: Continued.
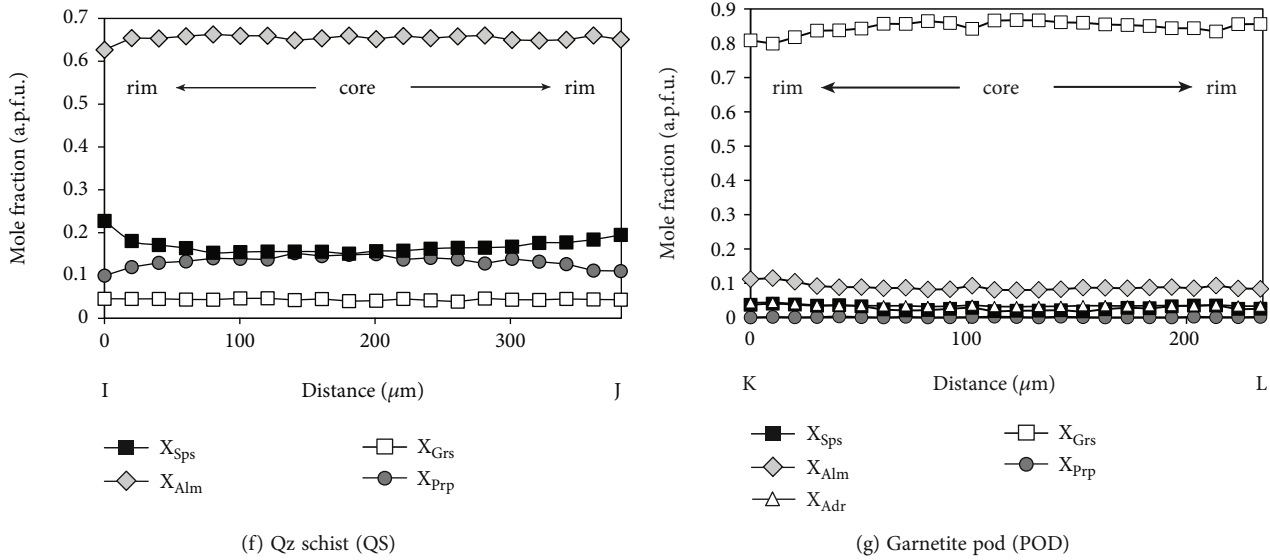
(f) Qz schist (QS)

(g) Garnetite pod (POD)

FIGURE 5: (a) Ternary diagram of garnet compositions in the pegmatites and schists. (b–g) Garnet end-member compositions (atoms per formula unit [apfu]) of the garnet profiles shown in Figure 6: (b) A–B in PgD, (c) C–D in PgC, (d) E–F in PgB, (e) G–H in BSa, (f) I–J in QS, and (g) K–L in POD. Note that the x-axis scale varies in each diagram.

(Figure 7(f)) are depleted in light REEs and have flat or slightly decreasing heavy REE patterns. Garnet ΣREE contents are high in the pegmatite samples and lower in the Bt and Qz schists (Figures 7(g) and 7(i)). The garnet ΣREE contents are highest in sample PgD (514–2770 ppm) and lower in samples PgC (103–2455 ppm) and PgB (260–1809 ppm; Table S1). The garnets in the schists and garnetite pod have lower ΣREE contents of 67–740, 107–284, and 18–40 ppm in samples BS, QS, and POD, respectively (Figures 7(g) and 7(i); Table S1).

All the garnets, apart from those in the garnetite pod, have negative Eu anomalies (Eu/Eu* < 1; Figure 7(g)), which decrease from the garnet in the pegmatites to that in the schists. Garnet in sample PgC has the largest negative Eu anomalies. Garnet in the garnetite pod has slightly positive Eu anomalies (Eu/Eu* > 1). The Sm and Gd contents of garnet are higher in the pegmatites than in the schists (Figure 7(h)), and thus, the garnet in the Bt schists exhibits higher REE fractionation than that in the pegmatites (Figure 7(h)). The ΣREE contents are strongly positively correlated with Y contents (Figure 7(i)). Garnet in the schist has low contents of heavy REEs, which are almost two orders of magnitude lower than the garnets in the pegmatites (Figures 7(a)–7(e) and 7(i)).

In some samples, the heavy REE contents in the garnets (or ΣREE contents) vary from core to rim. Garnet cores in samples PgD and PgC are enriched in heavy REEs (Figures 7(a) and 7(b)). Garnet in sample PgB shows increasing heavy REE contents in the Grs-rich region of irregular zoning (Figure 6(c)). The garnet with concentric zoning in the Bt schist sample (BSa) exhibits decreasing heavy REE contents from core to rim. However, garnet in sample BSb has relatively uniform heavy REE contents. The heavy REE contents of garnet in sample BSa are generally higher than those of garnet in sample BSb (Figure 7(i)). REE contents of garnet rims in sample PgB overlap with those of rims and cores in sample BSa (Figure 7(i)). Garnet in sample BSb has heavy REE contents that overlap with those of rims in samples PgB and QS (Figure 7(i)). Garnet in sample POD has higher contents of heavy REEs in high-Ti parts of the garnet grains (Figure 6(f)).

6.2. Other Trace Elements. Yttrium and Ti contents in the garnets are variable, and some garnets exhibit clear zonation (Figure 6). The garnet Y contents are correlated with REE abundances (Figure 7(i)) and are higher in the pegmatites than in the schists and garnetite pod. The highest Y contents are in garnets in samples PgD (1335–4650 ppm) and PgC (146–4850 ppm; Table S1), and garnets in sample PgC exhibit more heterogeneous Y zoning as compared with those in sample PgD. Garnet in the Bt-schist-hosted pegmatite (sample PgB) has lower Y contents of 577–2180 ppm. The pegmatite-hosting Bt schist (sample BS) has higher Y contents of 137–1160 ppm than the other schists (82–341 and 15–52 ppm for samples QS and POD, respectively; Table S1). Yttrium and Ti contents of the garnets exhibit a positive correlation, except for the garnetite pod that has lower Y and higher Ti contents as compared with its surrounding rock (sample QS) (Figure 7(j)).

Garnet in the pegmatites exhibits distinct zonation of Y and Ti. Garnet in sample PgD exhibits a marked decrease in Ti and Y contents at the rims (Figure 6(a)) and high-Ti sector zoning throughout the grains (Figure 6(a)). The garnets in sample PgC exhibit concentric oscillatory zoning of Ti and distinct sector zoning of Y (Figure 6(b)). Garnet in sample PgB exhibits slight zoning, particularly for Ti (Figure 6(c)), which is similar to the Ca zoning (Figure 6(c)). Garnet in the Bt schist has uniform Ti and Y contents, with some Y-rich areas in parts of the garnet rims (Figure 6(d)). Garnets in the sample POD exhibit irregular compositional zoning, particularly in Ti (Figure 6(f)).
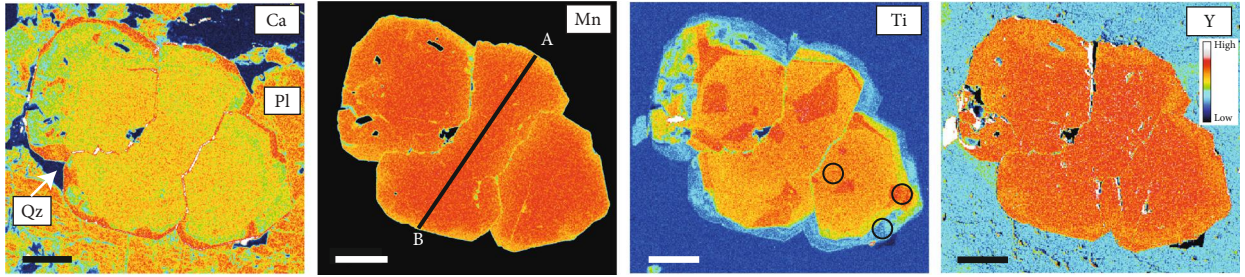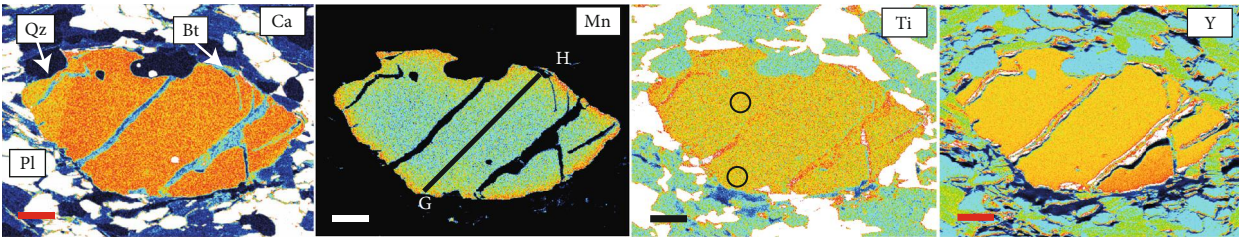
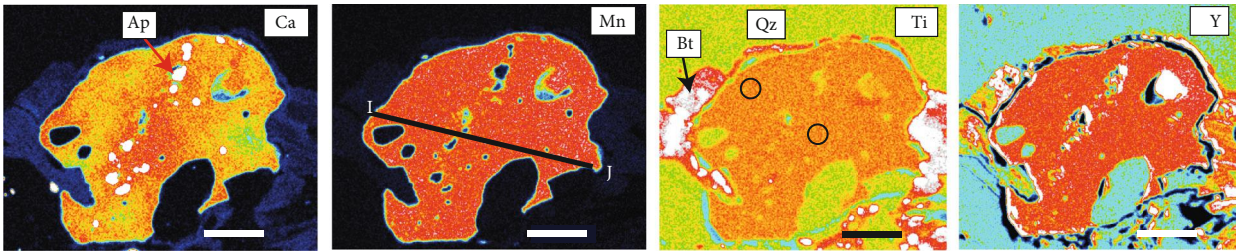(a) Garnet in Qz diorite-hosted pegmatite (PgD)
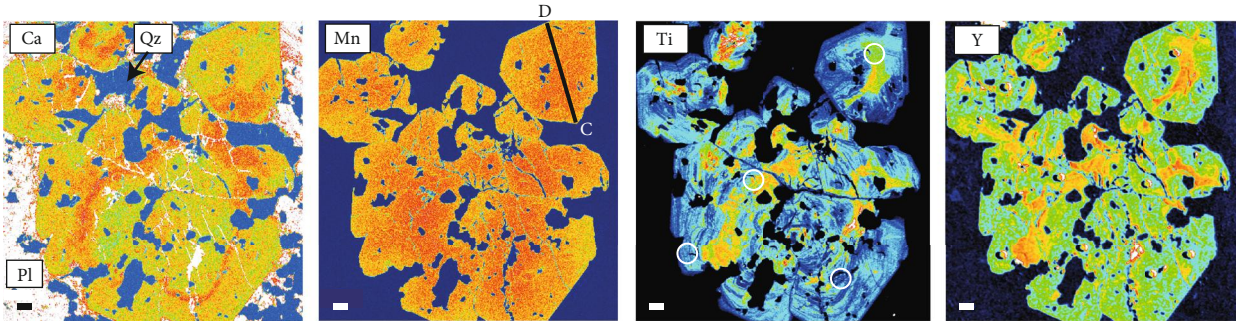
(b) Garnet in Cpx schist-hosted pegmatite (PgC)
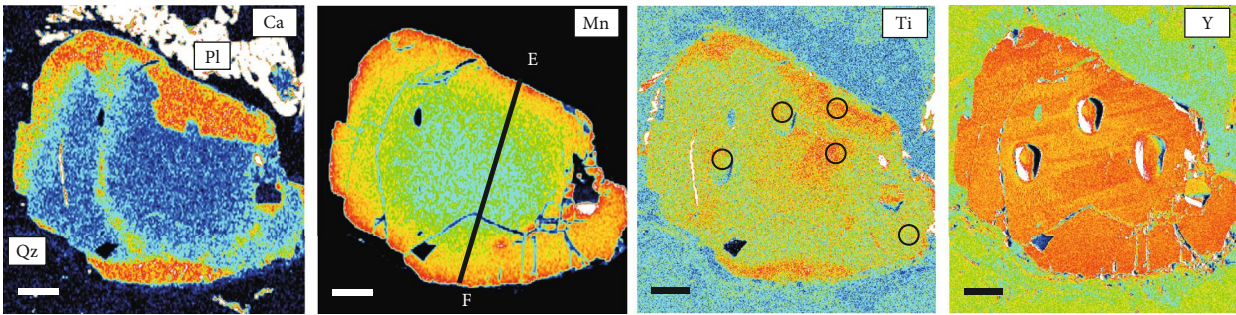
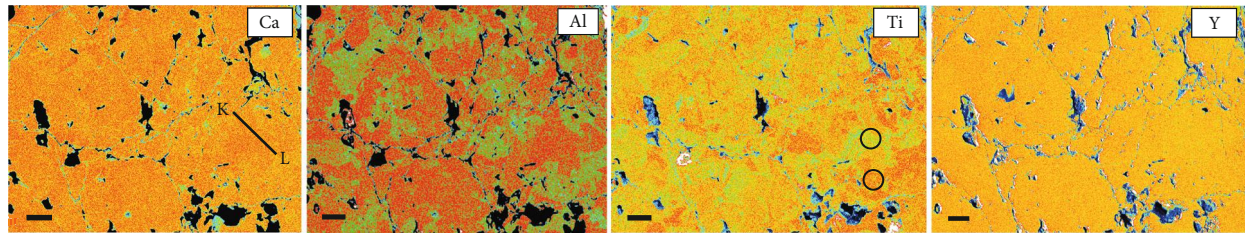(c) Garnet in Bt schist-hosted pegmatite (PgB)

(d) Garnet in Bt schist (BSa)

(e) Garnet in Qz schist (QS)

FIGURE 6: Continued.

(f) Garnetite pod (POD)

FIGURE 6: Representative examples of major and trace element (Y and Ti) zoning in garnet. (a) Garnet in a pegmatite (PgD) showing increasing Ca and decreasing Mn from core to rim along profile A–B (Figure 5(b)). The garnet exhibits Ti enrichment in its core and sector zoning and a slight decrease in Y from core to rim. (b) The garnet in PgC exhibits similar zoning of Mn as that in PgD, but also sector zoning of Ca and trace elements, and oscillatory zoning of Ti. (c) The garnet in PgB exhibits similar Ca zoning and the opposite Mn zoning as that in PgD, moderate Ti zoning, and no zoning of Y. The holes in the middle of the garnet are laser ablation pits. (d) A single garnet grain in a Bt schist (BSa) that is mostly unzoned. (e) Garnet in a Qz schist (QS) that has a Ca-rich core as compared with its rim and has uniform Mn, Ti, and Y contents (i.e., it is unzoned). (f) Garnetite pod with irregular zoning of Al and Ti and uniform Ca and Y contents. The scale bar is $100\,\mu$m long. Ap: apatite; Bt: biotite; Grt: garnet; Pl: plagioclase; Qz: quartz. The black or white open circles on the Ti maps are the sites of laser ablation analyses.

7. *P–T* Conditions of Pegmatite Formation and Metamorphism

To estimate the *P–T* conditions of garnet growth in the Bt schist, Qz schist, and pegmatites, Grt–Bt (GB) geothermometry [44] and Grt–Bt–Pl–Qz (GBPQ) geobarometry [45] were applied. The GB and GBPQ thermobarometers were calibrated for metamorphic pelites [44, 45], and caution is required when applying these to (meta-)igneous rocks [46]. In this study, the Bt and Qz schists are metamorphic in origin, whereas the mineral assemblages in the pegmatites were formed during crystallization in a magmatic–hydrothermal system. Given that the GBPQ geobarometer requires plagioclase compositions of $X_{An} > 0.17$, garnet compositions of $X_{Grs} > 0.03$, and biotite compositions of $X_{Al,Bt}$ ($Al^{VI}/[Fe^{2+} + Mg + Al^{VI} + Ti]) > 0.03$, its application was limited to the Bt schists (samples BSa and BSb) and the one pegmatite hosted by a Bt schist (sample PgB). PgB is not metamorphic in origin, but the chemical compositions of its minerals are similar to those of minerals in metamorphic rocks (i.e., Bt schists; Figure 4; Table 1), which allows GB and GBPQ thermobarometry to be used. Based on microstructural observations, we assumed that the garnet cores were in equilibrium with plagioclase and biotite cores (Table 2). A range of estimated *P–T* conditions was obtained due to the choice of mineral pairs within single samples. The estimated *P–T* conditions are 630–660°C at 0.20–0.39 GPa for the pegmatite sample PgB and 600–650°C at 0.27–0.41 GPa for the Bt schist (Figure 8(c)). These *P–T* conditions are slightly lower in temperature than for the crystallization of the quartz diorite (670–760°C) but are similar in pressure (0.30–0.45 GPa; [24]).

8. Fluid Inclusion Analyses

Fluid inclusions were analyzed in quartz grains from the pegmatite samples. Primary and secondary two-phase aqueous fluid inclusions occur in quartz grains. In all the pegmatite samples, primary fluid inclusions are rare as compared with the abundant secondary fluid inclusions (Figure 8(a)) and show rectangular, elongate, or irregular shapes. The size of the fluid inclusions ranges from 0.5 to $4.5\,\mu$m (average = $2.0 \pm 0.8\,\mu$m; Figure 8(a)). Assuming the area is equivalent to the volume proportion of the inclusion, the volume fraction of vapor is 12–15%. The homogenization temperatures of 31 fluid inclusions in pegmatites hosted by the Qz-diorite (sample PgD) are 205–360°C for primary fluid inclusions and 135–270°C for secondary fluid inclusions. The primary fluid inclusions in samples PgC and PgB have homogenization temperatures of 252–376°C and 236–288°C, respectively, and 138–216°C for secondary fluid inclusions in sample PgB (Figure 8(b)). The primary and secondary inclusions in the pegmatites have homogenization temperatures of 205–376°C and 135–270°C, respectively. Due to the small size of the fluid inclusions, the ice melting temperatures were only measured for sample PgB. The average ice-melting temperature is −2.4°C, which corresponds to a low salinity of ~4 wt.% NaCl$_{equivalent}$ [47]. The density of the primary inclusions varies between 0.57 and 0.89 g/cm^3.

The isochore ranges of the primary and secondary fluid inclusions are shown in Figure 8(c), which assumes a salinity of 4 wt.% NaCl$_{equivalent}$. Assuming the pressure was 0.30–0.45 GPa and the same as for the quartz diorite [24], the temperatures of fluid trapping within the pegmatites hosted by the Qz diorite, Cpx schist, and Bt schist show a wide range from ~400°C to a temperature close to that of crystallization of the quartz diorite (~760°C; Figure 8(c)).

9. Discussion

9.1. Timing and P–T Conditions of Garnet Growth. The Bt schists show that the *P–T* conditions of garnet growth were 600–650°C at 0.27–0.41 GPa which are similar to that determined by Endo et al. [32] (Figure 8(c)). It is also similar to or slightly lower than those of the crystallization of the Qz diorite (670–760°C and 0.30–0.45 GPa) [24, 32] and similar to those of the earlier stage of pegmatitic fluids (i.e., Na-rich fluid infiltration; [24]). Nurdiana et al. [24] showed that
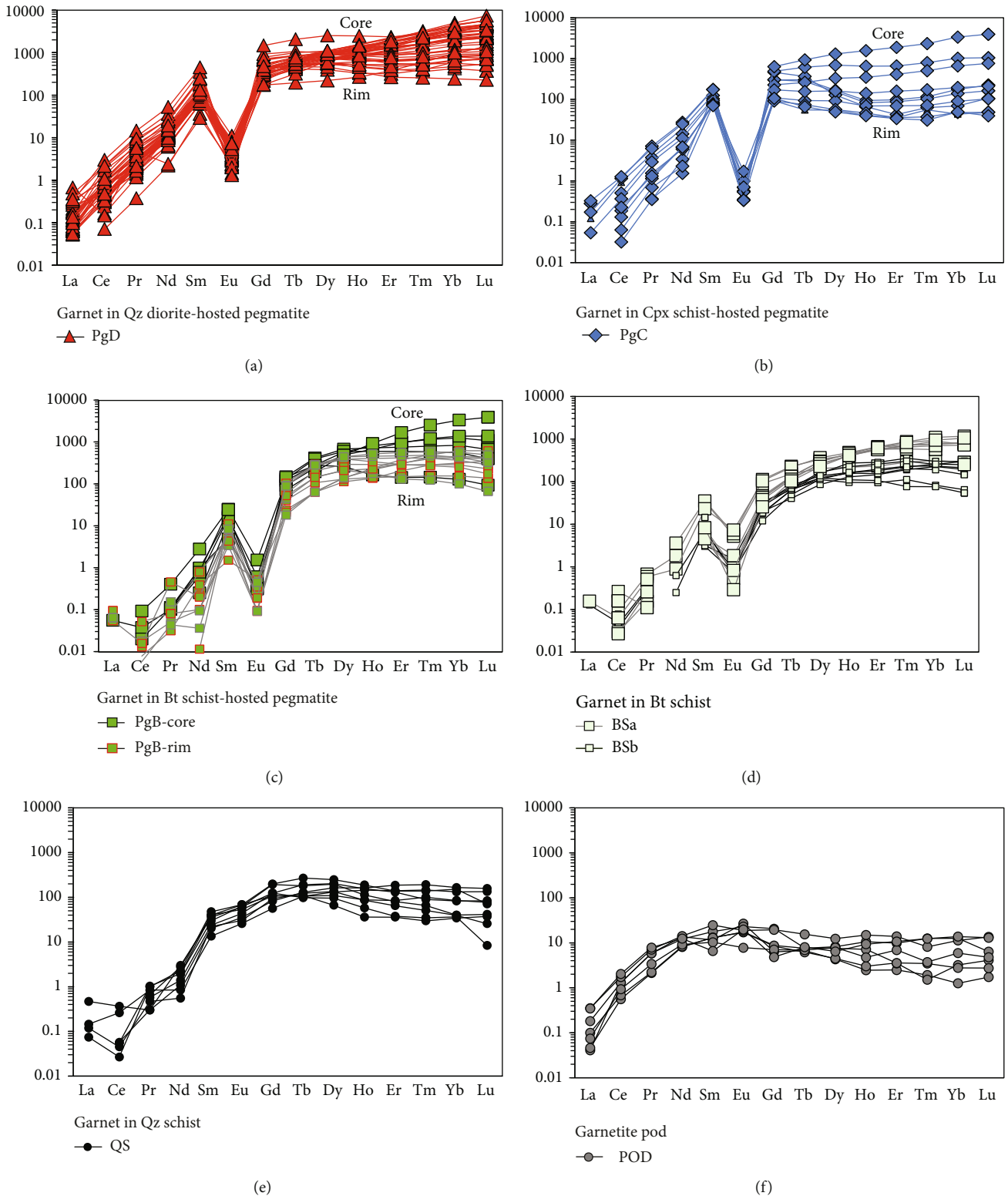
(a)

Garnet in Qz diorite-hosted pegmatite

(b)

Garnet in Cpx schist-hosted pegmatite

(c)

Garnet in Bt schist-hosted pegmatite

(d)

Garnet in Bt schist

(e)

Garnet in Qz schist

(f)

Garnetite pod
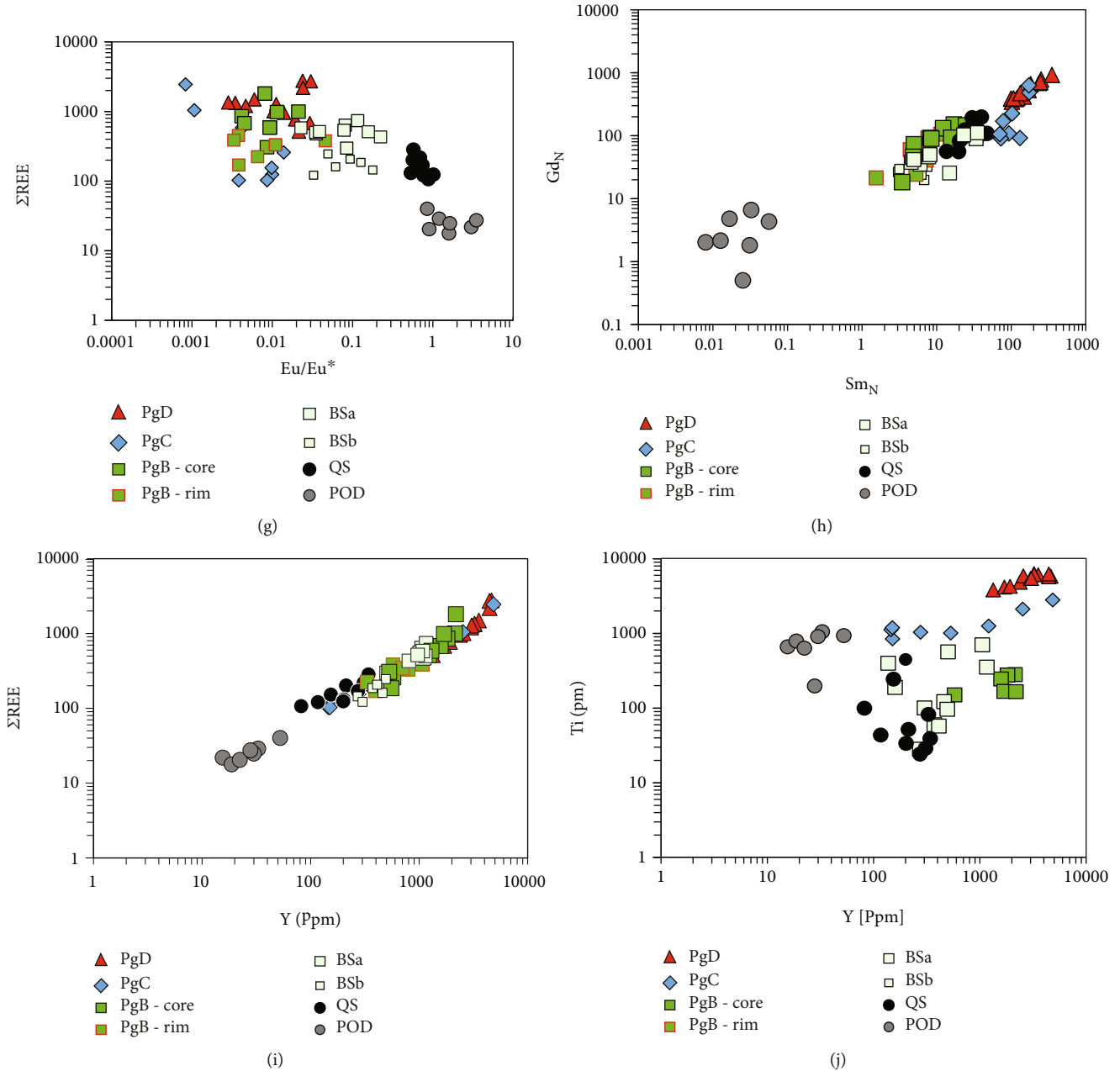
Figure 7: Continued.

(g)

(h)

(i)

(j)

Figure 7: Chondrite-normalized rare earth element (REE) patterns of garnet. (a) PgD, (b) PgC, (c) PgB, (d) BS, (e) QS, and (f) POD. The core compositions are generally more REE enriched than the rim compositions. For the BS, different samples are shown. La to Sm and Gd to Lu are referred to as the light and heavy REEs, respectively. (g) Eu/Eu* versus total REE contents. (h) Sm_N versus Gd_N. Sm_N and Gd_N are the chondrite-normalized concentrations of Sm and Gm, respectively. (i) Y versus total REE contents. (j) Y versus Ti. Chondrite-normalizing values are from Taylor and McLennan [39]. Note that the x-axis scale varies in (g–j).

crystallization of the quartz diorite was followed by two stages of fluid infiltration of pegmatitic fluids during cooling of the pluton (Figure 8(c)). The development of reaction zones around the pegmatite hosted by the Cpx schist indicates that the fluids released from the pegmatite caused the reactions in the surrounding metamorphic rocks (Figure 2(b)), although garnet is absent in the reaction zone [24]. In addition, we did not find any distinct zoning in garnet that could represent polyphase metamorphism (Figure 6(d)), and as such, garnet growth in the Bt schists

is inferred to have occurred during a single metamorphic event in response to intrusion of the Qz diorite into the relatively shallow crust as suggested by Endo et al. [32].

In the pegmatites, garnet commonly occurs with quartz in the central part of the dikes, suggesting that garnet formed at a relatively late stage [24]. Unfortunately, GB and GBPQ geothermobarometry cannot be applied to pegmatite samples (except for PgB), quartz schist, and garnetite pod. However, as discussed in the next section, the similarity in the garnet compositions of the pegmatite and adjacent Bt schist,
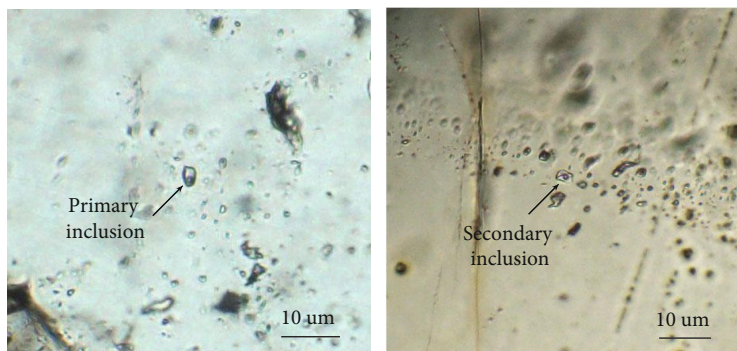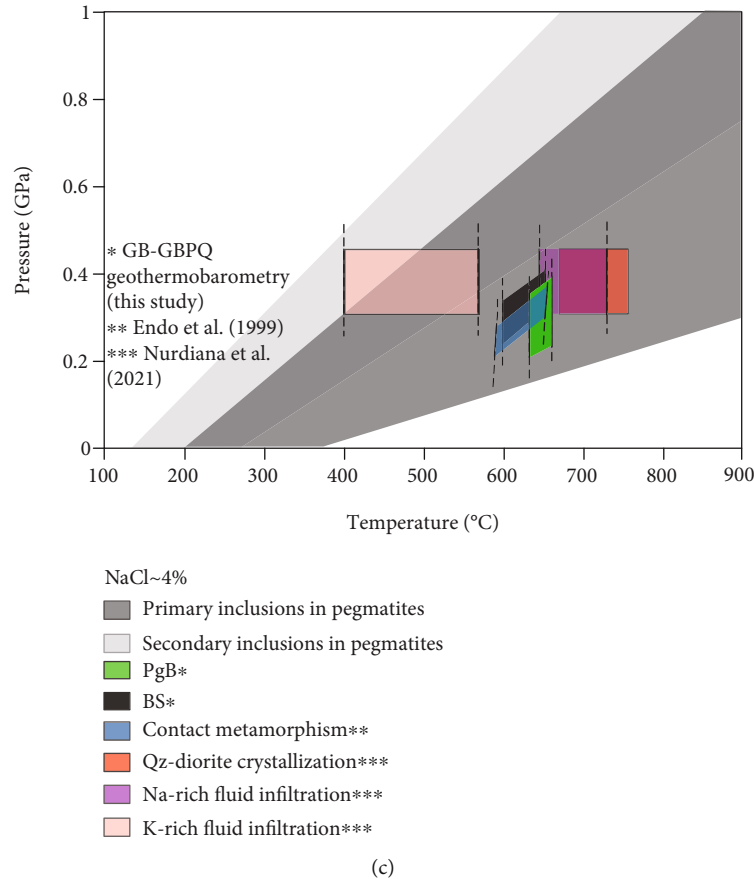
(a)
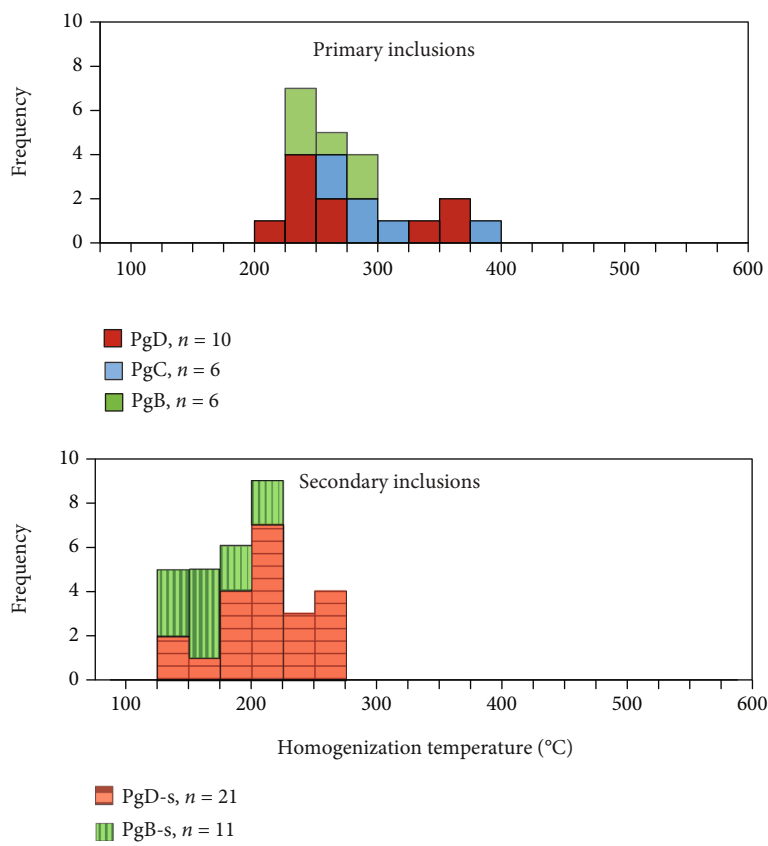
(b)

Figure 8: Continued.

FIGURE 8: Pressure–temperature conditions of quartz diorite crystallization, biotite schist metamorphism, and pegmatite infiltration. (a) Photomicrograph of fluid inclusions at room temperature. Two-phase primary inclusions and a planar array of secondary fluid inclusions occur in quartz in sample PgD. (b) Measured homogenization temperatures of fluid inclusions in quartz in the pegmatites. (c) Conditions of pegmatite formation as indicated by the shaded area from the isochores of the homogenization temperature range. The metamorphic conditions are based on GB and GBPQ geothermobarometry. The conditions of quartz diorite crystallization and pegmatite infiltration are from Nurdiana et al. [24]. PgD: Qz diorite-hosted pegmatite primary inclusions; PgD-s: Qz diorite-hosted pegmatite secondary inclusions; PgC: Cpx schist-hosted pegmatite primary inclusions; PgB: Bt schist-hosted pegmatite primary inclusions; PgB-s: Bt schist-hosted pegmatite secondary inclusions.

and garnetite pod and adjacent Qz schist, suggests that the garnet in the Bt and Qz schists grew at the same times as the garnet in the pegmatites.

The primary fluid inclusions in the quartz grains in the pegmatite samples had higher temperatures (200–380°C) than the secondary fluid inclusions (130–270°C) (Figure 8(b)). The homogenization temperatures of the primary fluid inclusions in pegmatite in the Bt schist (sample PgB) are concentrated from 230°C to 290°C. Assuming a pressure of 0.30–0.45 GPa and salinity of 4 wt.% NaCl$_{equivalent}$, the range of temperatures is 500–700°C, which is consistent with that from hornblende–plagioclase thermometry [24]. However, the number of fluid inclusions in the pegmatites hosted by the Qz diorite and Cpx schist is small, and the homogenization temperatures of the primary inclusions are more variable (200–360°C and 260–380°C, respectively). Some of the high homogenization temperatures (>350°C) are higher than the solidification temperature of the Qz diorite (Figure 8(c)). The reason for this is unclear, but these inclusions were possibly trapped at a fluid pressure lower than the lithostatic

pressure or were affected by volume change due to plastic deformation of the quartz [48] or experienced an implosion event [49].

The abundant secondary fluid inclusions in the pegmatites yielded temperatures of ~300–650°C at 0.30–0.45 GPa, which is consistent with the temperatures during the infiltration of K-rich fluid. This means that the pegmatite dikes acted as the dominant fluid pathway, even after the main stage of pegmatite crystallization.

9.2. Comparison of Garnet Compositions in the Pegmatites and Metamorphic Rocks. Three types of garnet have been reported in relation to intrusions with pegmatite dikes: igneous garnet in the pluton, igneous garnet in aplites and pegmatites, and metamorphic garnet in the surrounding metamorphic rocks [22, 50]. In this study, garnet was not found in the Qz diorite, but garnet in the pegmatites and metamorphic rocks has characteristic features in terms of compositional zoning and major element (Figure 5) and trace element (Figure 7) compositions. Garnet compositions

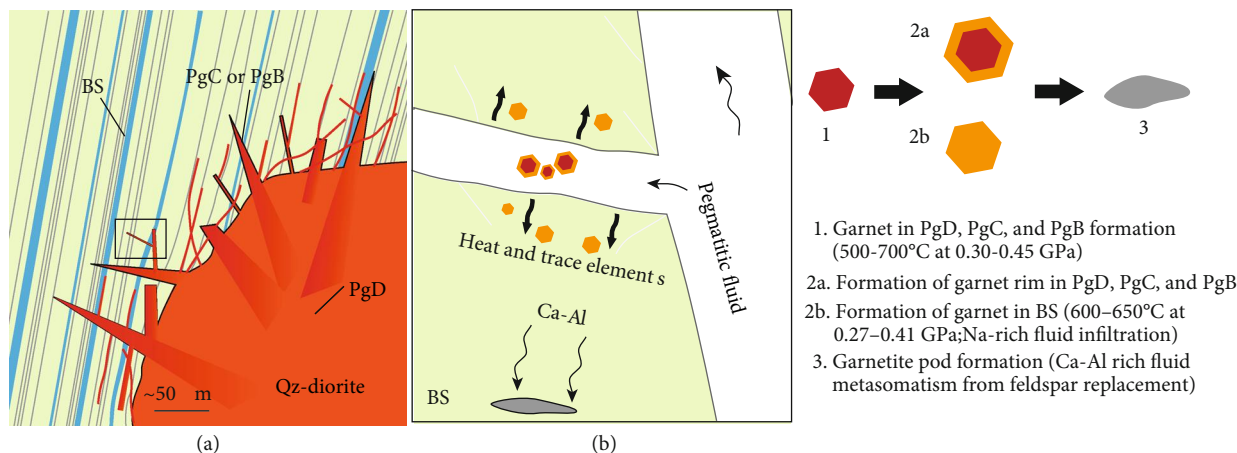(a)   (b)

FIGURE 9: Schematic model of fluid infiltration during pegmatite formation in the quartz diorite pluton and the surrounding metamorphic rocks. The fluid infiltration and trace element influx are recorded by the garnet texture and chemistry. The infiltration of Na-rich fluid resulted in the formation of Ca-rich rims and sector zoning in garnets in the pegmatites, and heavy-REE-rich garnets in the biotite schist, which was then followed by infiltration of K-rich fluids. Both fluids resulted in Ca–Al metasomatism. PgD: Qz diorite-hosted pegmatite; PgC: Cpx schist-hosted pegmatite; PgB: Bt schist-hosted pegmatite; BS: Bt schist; QS: Qz schist; POD: garnetite pod.

can be affected by the presence of coexisting biotite [46]. Although the trace element compositions of biotite were not analyzed in this study, the heavy REE compositions of garnet measured in this study (Figure 7) are higher than those for the Grt–Bt-bearing metamorphic and igneous rocks reported by Samadi et al. [46]. This means that garnet was the dominant host of heavy REEs in the Bt schists and pegmatite. In addition, the analyzed pegmatites and schists always contain biotite, and thus, the absence/presence of biotite is not the main control on the major and trace element variations (Figures 5–7).

Garnets in samples PgD and PgC (Figures 6(a) and 6(b)) typically exhibit concentric bell-shaped zoning in Mn, with some sector zoning. A reaction zone of replacement of clinopyroxene and Ca-rich plagioclase by hornblende and Na-rich plagioclase is developed around the pegmatite in sample PgC (Figure 2(b)), indicating that element transfer (e.g., Na and Si) into the crust occurred during the growth of garnet in this sample [24]. Garnet in the Bt schist and related pegmatite exhibits slight reverse zoning of Mn (Figures 6(c) and 6(d)), indicating reequilibration with biotite or diffusional modification during cooling (Figure 7). The Sps content of garnet shows a systematic decrease away from the pegmatite (Sps_{38-48}) hosted by the Qz diorite (sample PgD) to that in the pegmatite hosted by metamorphic rocks (Sps_{14-22}). Manganese-rich garnet in pegmatites has been reported in previous studies of natural aplites and pegmatites, which contain MnO > 12 wt.% and CaO < 2 wt.% [21, 22, 51]. On Kinkasan Island, some of the garnets in pegmatites hosted by the biotite schist have similar Sps contents in the pegmatite (sample PgB) and adjacent schist (sample BS; Figure 5(a)), suggesting that garnet growth in the Bt schists occurred during fluid infiltration from the pegmatites.

Garnet in the Qz schist (sample QS) has major element compositions similar to the Alm-rich compositions in samples PgB and BS (Figure 5(a)). The garnet in the Qz schist has lower REE and Ti contents than those in the pegmatites

(Figures 7(g), 7(i), and (j)). Garnet in the garnetite pod (sample POD) has high Grs contents (Figure 5(a)) and relatively high Ti contents similar to those in samples PgC and PgB (Figure 7(j)).

Chondrite-normalized REE patterns of garnets in the pegmatites and Bt schist (Figures 7(a)–7(d)) are typical igneous garnet, which is characterized by enrichment of heavy REEs [52] and negative Eu anomalies. The negative Eu anomalies are more evident in the plagioclase-bearing pegmatites (samples PgD, PgC, and PgB; Figures 7(a)–7(c)) and schists (sample BS; Figure 7(d)), whereas the negative Eu anomalies are small or absent in the plagioclase-free samples (QS and POD; Figures 7(e) and 7(f)). This indicates that the formation of plagioclase caused the negative Eu anomalies in the garnets [53]. The occurrence of garnet grains with Eu anomalies in the center of the pegmatite dikes shows that garnet growth occurred along with plagioclase growth during the late stages of pegmatite crystallization.

Garnets in pegmatites and schists analyzed in previous studies [22, 54] exhibit heavy REE contents that are highly variable. Garnet in pegmatites has high heavy REE contents of 1000–10,000 ppm, whereas garnet in pelitic schist has lower heavy REE contents of 10–100 ppm. In this study, the heavy REE contents of garnets in the schists are highly variable, and the highest contents are similar to those of garnets in the pegmatites or other veins (e.g., samples BSa and PgB; Figures 7(i) and 7(j)). However, garnet in sample BSb, which was collected farther from the pegmatite, has lower contents of heavy REEs as compared with that in sample BSa. This indicates that the high contents of heavy REEs in garnets in the Bt schist resulted from fluid infiltration from the pegmatites (Figure 9).

In summary, the trace element data for the studied garnets identifies three groupings: (1) pegmatitic garnet in sample PgD that is Mn-rich and (heavy) REE-rich and has negative Eu anomalies; (2) Fe-rich garnet in sample BS with lower REE contents and a similar pattern of heavy REE and

Eu anomalies to pegmatitic garnet (note that garnets in samples PgC and PgB are intermediate between (1) and (2)); and (3) Ca–Ti-rich garnet in the garnetite pod (sample POD) and adjacent quartz schist (QS), which has the lowest REE contents, flat or slightly depleted heavy REE patterns, and small positive Eu anomalies.

9.3. Trace Element Fractionation and Fluid Transfer in the Contact Aureole.
The pegmatite hosted in the Bt schist (sample PgB) is in contact with the Bt schist sample BS (Figure 2(c)). The heavy REE contents of the garnets in the Bt schist (sample BS) are as high as in the garnet rims in the pegmatite (sample PgB). The garnet in sample BSa occurs only along the boundary with the pegmatite and exhibits the same Mn zoning as those in sample PgB. Therefore, the relatively high REE contents of garnet in the Bt schist (Figure 7(d)) could not have been formed by solidification of melt but instead formed by infiltration of REE-rich fluid from the pegmatite dikes. The pegmatite PgB is relatively thin (3–5 cm wide), and it is possible that the similar compositions of PgB and BSa are due to postcrystallization modification of REE contents in garnet in the pegmatite by diffusive exchange with the host Bt schist. However, postcrystallization modification involving centimeter-scale diffusion is unlikely, as the duration of high temperatures (>600°C) after intrusion would have been as short as <0.5 Myr, as constrained by analyses of the contact metamorphic rocks with similar P-T condition around granite intrusions in the Ryoke metamorphic belt [17].

The plagioclase anorthite content is lower in sample PgD than in samples PgC and PgB (Figure 4(a)). The garnet REE and Y contents of garnet in the pegmatites exhibit a systematic decrease from the Qz diorite (sample PgD) to the Cpx schist (sample PgC) to the Bt schist (sample PgB). This could be due to several factors, including the initial melt composition, magma fractionation, and/or fluid accumulation during crystallization [22, 55, 56]. The Qz diorite on Kinkasan Island is a plutonic body with a simple structure, and it is unlikely that each pegmatite was derived from a different parental magma. As such, fractionation of fluids in a magmatic-hydrothermal system during the formation of a series of pegmatites best explains the decreasing Y and REE contents in the garnets, with the most fractionated pegmatite (sample PgB) having lower REE contents. The REE-poor garnet rims may be related to fluid activity [56]. Decreasing REE contents from sample PgD to PgB suggest an increase of volume of aqueous fluids in the system, which underwent cooling and changes in Ca and Na contents.

The Grs-rich garnet in the garnetite pod (sample POD) is characterized by the lowest heavy REE contents of all the samples (Figures 7(f)–7(i)). The low contents of heavy REEs could be due to the following: (1) a heavy REE-depleted protolith, (2) the precipitation of unobserved heavy REE-rich minerals, or (3) the effects of heavy REE-depleted fluid infiltration. A heavy REE-depleted protolith is unlikely, as the Qz schists surrounding the garnetite pod contain garnet with high contents of heavy REEs. In addition, minerals rich in heavy REEs were not identified in at least three thin sections of the sample POD. The formation of Grs-rich garnet in

samples QS and POD is indicative of the infiltration of Ca-rich aqueous fluids. Such Grs-rich garnetite pods have been reported in previous studies of anorogenic and orogenic granitic pegmatites [57, 58]. The replacement of An_{9-55} plagioclase by albite in the pegmatites is called a "back-reaction" [57], which provides an internal source for Ca-metasomatism [58] that results in autometasomatism of primary minerals in pegmatites [21]. On Kinkasan Island, one plausible source of Ca to produce the garnetite pod is leaching of sodic plagioclase during the replacement of plagioclase in the mafic schists [24]. For example, replacement of the Cpx schists by Na-rich plagioclase and hornblende was induced by Na-rich fluid infiltration from the pegmatites at 690–730°C and 0.30–0.45 GPa, which caused gains of Na_2O (0.83%) and H_2O (0.30%) and loss of CaO (3.17%) for every 100 g of unaltered wall rock [24]. The dissolution of An-rich plagioclase is consistent with the absence of a negative Eu anomaly, given that Eu ion behaves similarly to Ca ion.

Variations of Ti and Y contents in garnet and zoning can be produced by changes in P-T conditions, open system fluid infiltration, or the presence of Ti- or Y-enriched phases [18, 59]. The oscillatory zoning of Ti in the garnets in the pegmatites (Figure 6(b); sample PgC) is indicative of open system behavior of the fluid circulation system, as suggested by Jamtveit et al. [18]. Titanium- or Y-bearing minerals could affect the garnet compositions, because the pegmatites contain Ti- and Y-bearing accessory minerals such as ilmenite (~52 wt.% TiO_2), zircon (~6 wt.% Y_2O_3), and monazite-(Ce) (~3 wt.% Y_2O_3).

During fractional crystallization of pegmatites, H_2O-rich and -poor melts can coexist [60]. H_2O-rich melt may contain ~40 wt.% H_2O, is rich in alkaline elements, and becomes a mobile phase [8, 60]. On Kinkasan Island, the pegmatitic fluids that caused alteration in the crust were characterized by two compositions (i.e., Na- and K-rich aqueous fluids). The source of these Na- and K-rich aqueous fluids was probably H_2O-rich melts that formed during fractionation of the pegmatites [21, 61].

A possible model showing the relationships between the pegmatitic fluid activity, alteration, and garnet growth is summarized in Figure 9. During the formation of large pegmatite dikes, the pegmatite cores had higher H_2O activity as compared with their margins [51], and thus, garnet formation occurred in the H_2O-rich melts or aqueous fluids (Figure 9(a)). The infiltration of Na-rich aqueous fluids from the pegmatites into the crust [24] probably occurred during the main stage of garnet growth in the pegmatites at 500–700°C and 0.30–0.45 GPa (Figure 9(b)). The infiltrations of Na-rich fluid resulted in the Ca-rich rims and sector zoning in the garnets in the pegmatites and heavy REE-rich garnet in the biotite schist (Figure 7) at 600–650°C and 0.27–0.41 GPa (Figure 8(c)). This was followed by the infiltration of K-rich fluid into the schist. Both fluid types infiltrated the mafic schist and resulted in a large loss of Ca (1.50–3.17 wt.%) and Al (~1.76 wt.%; [24]). These elements (i.e., Ca and Al) released during the alteration of the mafic schists migrated to other lithologies and produced the garnetite pods consisting of Grs-rich garnet (Figure 9(b)). This suggests

that open-system fluid circulation between granitic plutons and the crust controls the transfer of heat and mass that leads to alteration and/or metasomatism under low-temperature conditions.

10. Conclusions

The major and trace element compositions of garnets in pegmatites and schists on Kinkasan Island were determined to understand the element transport from the pluton into the middle crust.

(1) Garnets occur in both the pegmatites and adjacent metamorphic rocks and have a range of compositions. The garnets in pegmatites hosted by the Qz diorite have Sps-rich compositions of Sps_{57-69} $Alm_{22-30}Prp_{3-4}Grs_{3-10}$, whereas those in the Bt schist have Sps16–30Alm54–66Prp9–16Grs3–6. The garnets in pegmatites hosted by the metamorphic rocks (Bt and Cpx schists) have intermediate compositions ($Sps_{14-48}Alm_{44-70}Prp_{2-14}Grs_{1-13}$). In contrast, garnets in the garnetite pod hosted by Qz schist have a Grs-rich composition ($Sps_{1-4}Alm_{8-11}$ $Prp_{0.1-0.4}Grs_{80-87}$ Adr_{3-4})

(2) P–T conditions of garnet growth in the biotite schist during contact metamorphism were estimated to be 600–650°C at 0.27–0.41 GPa by GB and GBPQ geothermobarometry. The pegmatitic fluid infiltration into the biotite schist was constrained from fluid inclusion analysis to have occurred at 500–700°C, assuming the pressure was 0.30–0.45 GPa. These P–T conditions indicate that metamorphism and pegmatitic fluid infiltration occurred during pluton crystallization and the early stages of pegmatitic fluid infiltration (i.e., Na-rich fluids)

(3) Based on the trace element data, the garnets are divided into three groups. The first is pegmatitic garnet hosted by the quartz diorite, which has the highest REE contents (ΣREE > 4590 ppm) and negative Eu anomalies. The second is garnet in the Bt schist that has REE contents (ΣREE > 1080 ppm) that are two orders of magnitude lower than those of garnets in the pegmatites, but has similar heavy REE patterns and negative Eu anomalies. The garnet in the pegmatites hosted by the Bt and Cpx schists is intermediate between the first and second types of garnet. The third group is the Grs-rich garnet in the garnetite pod, which has the lowest REE contents (ΣREE = ~ 600 ppm), Ti-rich compositions, and no Eu anomalies

(4) The pegmatitic fluid was released during the late stages of granitic intrusion and resulted in several types of metamorphic and alteration processes. Garnet in the biotite schist near the pegmatites has similar trace element compositions as those in the pegmatites, suggesting that garnet growth in the schist was related to the infiltration of pegmatitic fluids. The feldspar alteration due to infiltration of Na- and K-rich fluids produced Ca–Al-rich fluids, which resulted in the formation of Grs-rich garnet in the garnetite pod. The slightly positive Eu anomalies of garnet in the garnetite pod is consistent with the breakdown of the anorthite component in plagioclase. Our results suggest that pegmatitic fluid enhances not only heat transport but also fluid and elemental transport into the middle crust

Data Availability

The major element and trace element compositions of garnet are presented in the main text and supplementary file, respectively.

Conflicts of Interest

The authors declare that they have no conflicts of interest.

Acknowledgments

Supplementary Materials

The supplementary material consists of one MS Word file containing Figure S1 and Table S1. Figure S1 is the chondrite-normalized trace element spider diagram of garnet in the study area. Table S1 is a list of representative trace element compositions of garnet in Kinkasan Island, including the ΣREE and Eu/Eu* values. *(Supplementary Materials)*

References

[1] A. K. Engvik, A. Bertram, J. F. Kalthoff, B. Stöckhert, H. Austrheim, and S. Elvevold, "Magma-driven hydraulic fracturing and infiltration of fluids into the damaged host rock, an example from Dronning Maud Land, Antarctica," *Antarctica. Journal of Structural Geology*, vol. 27, no. 5, pp. 839–854, 2005.

[2] T. John, N. Gussone, Y. Y. Podladchikov et al., "Volcanic arcs fed by rapid pulsed fluid flow through subducting slabs," *Nature Geoscience*, vol. 5, no. 7, pp. 489–492, 2012.

[3] M. Uno, A. Okamoto, and N. Tsuchiya, "Excess water generation during reaction-inducing intrusion of granitic melts into ultramafic rocks at crustal P-T conditions in the Sør Rondane Mountains of East Antarctica," *Lithos*, vol. 284-285, pp. 625–641, 2017.

[4] P. Černý, P. L. Blevin, M. Cuney, and D. London, *Granite-related ore deposits* Society of Economic Geologists..

[5] D. London, "Ore-forming processes within granitic pegmatites," *Ore Geology Reviews*, vol. 101, pp. 349–383, 2018.

[6] K. Okamoto, H. Asanuma, T. Ishibashi et al., "Geological and engineering features of developing ultra-high-temperature geothermal systems in the world," *Geothermics*, vol. 82, no. -January, pp. 267–281, 2019.

[7] N. Tsuchiya, R. Yamada, and M. Uno, "Supercritical geothermal reservoir revealed by a granite-porphyry system," *Geothermics*, vol. 63, pp. 182–194, 2016.

[8] R. Barros, D. Kaeter, J. F. Menuge, and R. Škoda, "Controls on chemical evolution and rare element enrichment in crystallising albite-spodumene pegmatite and wallrocks: constraints from mineral chemistry," *Lithos*, vol. 352-353, article 105289, 2020.

[9] S. Guillot, P. Le Fort, A. Pecher, M. R. Barman, and J. Aprahamian, "Contact metamorphism and depth of emplacement of the Manaslu granite (central Nepal). Implications for Himalayan orogenesis," *Implications for Himalayan orogenesis. Tectonophysics*, vol. 241, no. 1–2, pp. 99–119, 1995.

[10] D. D. Hickmott and N. Shimizu, "Trace element zoning in garnet from the Kwoiek area, British Columbia: disequilibrium partitioning during garnet growth?," *Contributions to Mineralogy and Petrology*, vol. 104, no. 6, pp. 619–630, 1990.

[11] H. H. Stowell, T. Menard, and C. K. Ridgway, "Ca-metasomatism and chemical zonation of garnet in contact metamorphic aureoles, Juneau gold belt," *Southeastern Alaska. Canadian Mineralogist*, vol. 34, no. 6, pp. 1195–1209, 1996.

[12] M. Enami, "Pressure-temperature path of Sanbagawa prograde metamorphism deduced from grossular zoning of garnet," *Journal of Metamorphic Geology*, vol. 16, no. 1, pp. 97–106, 1998.

[13] F. Gaidies, C. Capitani, R. Abart, and R. Schuster, "Prograde garnet growth along complex P–T–t paths: results from numerical experiments on polyphase garnet from the Wölz Complex (Austroalpine basement)," *Contributions to Mineralogy and Petrology*, vol. 155, no. 6, pp. 673–688, 2008.

[14] F. S. Spear, "Metamorphic phase equilibria and pressure–temperature–time paths," *Mineralogical Society of America Monograph.*, pp. 352–356, 1993.

[15] M. Uno, H. Iwamori, and M. Toriumi, "Transition from dehydration to hydration during exhumation of the Sanbagawa metamorphic belt, Japan, revealed by the continuous P–T path recorded in garnet and amphibole zoning," *Contributions to Mineralogy and Petrology*, vol. 170, no. 3, pp. 1–22, 2015.

[16] J. Ganguly, S. Dasgupta, W. Cheng, and S. Neogi, "Exhumation history of a section of the Sikkim Himalayas, India: records in the metamorphic mineral equilibria and compositional zoning of garnet," *Earth and Planetary Science Letters*, vol. 183, no. 3–4, pp. 471–486, 2000.

[17] T. Okudaira, "Temperature–time path for the low-pressure Ryoke metamorphism, Japan, based on chemical zoning in garnet," *Journal of Metamorphic Geology*, vol. 14, no. 4, pp. 427–440, 1996.

[18] B. Jamtveit, R. A. Wogelius, and D. G. Fraser, "Zonation patterns of skarn garnets: records of hydrothermal system evolution," *Geology*, vol. 21, no. 2, pp. 113–116, 1993.

[19] A. D. L. Skelton, "The effect of metamorphic fluid flow on the nucleation and growth of garnets from Troms, North Norway," *Journal of Metamorphic Geology*, vol. 15, no. 1, pp. 85–92, 1997.

[20] A. Skelton, H. Annersten, and J. Valley, "Delta18O and yttrium zoning in garnet: time markers for fluid flow?," *Journal of Metamorphic Geology*, vol. 20, no. 5, pp. 457–466, 2002.

[21] A. Müller, A. Kearsley, J. Spratt, and R. Seltmann, "Petrogenetic implications of magmatic garnet in granitic pegmatites from southern Norway," *Canadian Mineralogist*, vol. 50, no. 4, pp. 1095–1115, 2012.

[22] R. Samadi, N. R. Miller, H. Mirnejad, C. Harris, H. Kawabata, and N. Shirdashtzadeh, "Origin of garnet in aplite and pegmatite from Khajeh Morad in northeastern Iran: a major, trace element, and oxygen isotope approach," *Lithos*, vol. 208-209, pp. 378–392, 2014.

[23] T. Inoki, F. Takizawa, and M. Katada, "Some problems concerning the geotectonics of Kinkaza islet, Miyagi prefecture, Japan," *Earth Science*, vol. 26, pp. 139–148, 1972, (in Japanese with English abstract).

[24] A. Nurdiana, A. Okamoto, K. Yoshida, M. Uno, T. Nagaya, and N. Tsuchiya, "Multi-stage infiltration of Na- and K-rich fluids from pegmatites at mid-crustal depths as revealed by feldspar replacement textures," *Lithos*, vol. 388-389, article 106096, 2021.

[25] M. Ehiro, T. Tsujimori, K. Tsukada, and M. Nuramkhaan, "Palaeozoic basement and associated cover," *The Geology of Japan*, vol. 25–60, 2016.

[26] Y. Isozaki, M. Ehiro, H. Nakahata, K. Aoki, S. Sakata, and T. Hirata, "Cambrian plutonism in Northeast Japan and its significance for the earliest arc-trench system of proto-Japan: new U-Pb zircon ages of the oldest granitoids in the Kitakami and Ou Mountains," *Journal of Asian Earth Sciences*, vol. 108, pp. 136–149, 2015.

[27] N. Tsuchiya, J. I. Kimura, and H. Kagami, "Petrogenesis of Early Cretaceous adakitic granites from the Kitakami mountains, Japan," *Journal of Volcanology and Geothermal Research*, vol. 167, pp. 134–159, 2007.

[28] Y. Isozaki, K. Aoki, T. Nakama, and S. Yanai, "New insight into a subduction-related orogen: a reappraisal of the geotectonic framework and evolution of the Japanese Islands," *Gondwana Research*, vol. 18, no. 1, pp. 82–105, 2010.

[29] M. Kawamura, M. Kato, and Group, K P R, "Southern Kitakami terrane," in *Pre-Cretaceous Terranes of Japan (Eds)*, K. Ichikawa, S. Mizutani, I. Hara, S. Hada, and A. Yao, Eds., pp. 249–266, Nippon–Insatsu, Osaka, 1990, Retrieved from http://ci.nii.ac.jp/naid/10003770381/en/.

[30] F. Takizawa, N. Isshiki, and M. Katada, *Geology Sheet Map of the Kinkasan District with Explanatory Text: 1:50,000*, Geological Survey of Japan, 1974.

[31] T. Kobayashi, "The Sakawa orogenic cycle and its bearing on the origin of the Japanese Islands," *J. Fac. Sci., Imp. Univ. Tokyo, Sec.*, vol. 2, pp. 219–578, 1941.

[32] M. Endo, N. Tsuchiya, and J. Kimura, "Petrochemical characteristics and their geological implications of the Kinkasan granitic rocks, South Kitakami Belt, Japan," *Memory of Geological Society of Japan*, vol. 53, pp. 85–110, 1999, In Japanese with English abstract.

[33] N. Tsuchiya, T. Takeda, T. Adachi, N. Nakano, Y. Osanai, and K. Adachi, "Early Cretaceous adakitic magmatism and tectonics in the Kitakami Mountains, Japan," *Japanese Magazine of Mineralogical and Petrological Sciences*, vol. 44, no. 2, pp. 69–90, 2015, In Japanese with English abstract.

[34] Y. Kawano and Y. Ueda, "K–Ar dating on the igneous rocks in Japan (II) Granitic rocks in Kitakami massif," *The Journal of the Japanese Association of Mineralogists, Petrologists and Economic Geologists*, vol. 53, no. 4, pp. 143–154, 1965.

[35] Y. Ueda, K. Yamaoka, H. Onuki, and M. Tagiri, "K-Ar dating on the metamorphic rocks in Japan II," *The Journal of the*

Japanese Association of Mineralogists, Petrologists and Economic Geologists, vol. 61, no. 3, pp. 92–99, 1969.

[36] T. Abe and M. Katada, "Chemical composition of plutonic rocks in Northeast Japan 2. Kinkasan granites and metamorphic rocks," *Bulletin of the Geological Survey of Japan*, vol. 25, no. 10, pp. 517–523, 1974, (in Japanese with English abstract).

[37] A. J. Locock, "An Excel spreadsheet to recast analyses of garnet into end-member components, and a synopsis of the crystal chemistry of natural silicate garnets," *Computers and Geosciences*, vol. 34, no. 12, pp. 1769–1780, 2008.

[38] K. P. Jochum, U. Weis, B. Stoll et al., "Determination of reference values for NIST SRM 610–617 glasses following ISO guidelines," *Geostandards and Geoanalytical Research*, vol. 35, no. 4, pp. 397–429, 2011.

[39] S. R. Taylor and S. M. McLennan, *The Continental Crust: its Composition and Evolution*, Blackwell, Oxford, 1985.

[40] R. J. Bodnar, "Introduction to aqueous-electrolyte fluid systems," in *Fluid Inclusions: Analysis and Interpretation*, I. Samson, A. Anderson, and D. Marshall, Eds., pp. 81–99, Mineralogical Association of Canada, 2003, Short Course 32.

[41] Y. G. Zhang and J. D. Frantz, "Determination of the homogenization temperatures and densities of supercritical fluids in the system $NaClKClCaCl_2H_2O$ using synthetic fluid inclusions," *Chemical Geology*, vol. 64, no. 3-4, pp. 335–350, 1987.

[42] R. J. Bakker, "Package FLUIDS 1. Computer programs for analysis of fluid inclusion data and for modelling bulk fluid properties," *Chemical Geology*, vol. 194, no. 1-3, pp. 3–23, 2003.

[43] M. Rieder, G. Cavazzini, Y. S. D'yakonov et al., "Nomenclature of the micas," *Clays and Clay Minerals*, vol. 46, no. 5, pp. 586–595, 1998.

[44] M. J. Holdaway, "Application of new experimental and garnet Margules data to the garnet-biotite geothermometer," *American Mineralogist*, vol. 85, no. 7-8, pp. 881–892, 2000.

[45] C. Wu, J. Zhang, and L. Ren, "Empirical garnet–biotite–plagioclase–quartz (GBPQ) geobarometry in medium- to high-grade metapelites," *Journal of Petrology*, vol. 45, no. 9, pp. 1907–1921, 2004.

[46] R. Samadi, G. Torabi, H. Kawabata, and N. R. Miller, "Biotite as a petrogenetic discriminator: chemical insights from igneous, meta- igneous and meta-sedimentary rocks in Iran," *Lithos*, vol. 386-387, article 106016, 2021.

[47] D. L. Hall, S. M. Sterner, and R. J. Bodnar, "Freezing point depression of NaCl-KCl-H_2O solutions," *Economic Geology*, vol. 83, no. 1, pp. 197–202, 1988.

[48] L. W. Diamond, A. Tarantola, and H. Stünitz, "Modification of fluid inclusions in quartz by deviatoric stress. II: experimentally induced changes in inclusion volume and composition," *Contributions to Mineralogy and Petrology*, vol. 160, no. 6, pp. 845–864, 2010.

[49] M. O. Vityk and R. J. Bodnar, "Textural evolution of synthetic fluid inclusions in quartz during reequilibration, with applications to tectonic reconstruction," *Contributions to Mineralogy and Petrology*, vol. 121, no. 3, pp. 309–323, 1995.

[50] R. Samadi, H. Mirnejad, H. Kawabata, C. Harris, M. V. Valizadeh, and E. Gazel, "Magmatic garnet in the Triassic (215 Ma) Dehnow pluton of NE Iran and its petrogenetic significance," *International Geology Review*, vol. 56, no. 5, pp. 596–621, 2014.

[51] E. H. Arredondo, G. R. Rossman, and G. R. Lumpkin, "Hydrogen in spessartine-almandine garnets as a tracer of granitic pegmatite evolution," *American Mineralogist*, vol. 86, no. 4, pp. 485–490, 2001.

[52] C. S. Schwandt, J. J. Papike, C. K. Shearer, and A. J. Brearley, "A Sim investigation of REE chemistry of garnet in garnetite associated with the Broken Hill Pb-Zn-Ag orebodies, Australia," *Australia. Canadian Mineralogist*, vol. 31, no. 2, pp. 371–379, 1993.

[53] A. Heimann, P. G. Spry, G. S. Teale, C. H. H. Conor, and N. J. Pearson, "The composition of garnet in garnet-rich rocks in the southern Proterozoic Curnamona Province, Australia: an indicator of the premetamorphic physicochemical conditions of formation," *Mineralogy and Petrology*, vol. 101, no. 1-2, pp. 49–74, 2011.

[54] A. El Korh, S. T. Schmidt, A. Ulianov, and S. Potel, "Trace element partitioning in HP–LT metamorphic assemblages during subduction-related metamorphism, Ile de Groix, France: a detailed LA-ICPMS study," *Journal of Petrology*, vol. 50, no. 6, pp. 1107–1148, 2009.

[55] S. Smeds, "Zoning and fractionation trends of a peraluminous NYF granitic pegmatite field at Falun, south–central Sweden," *GFF*, vol. 116, no. 3, pp. 175–184, 1994.

[56] R. C. Wang, F. Fontan, X. M. Chen et al., "Accessory minerals in the Xihuashan Y-enriched granitic complex, southern China: a record of magmatic and hydrothermal stages of evolution," *Canadian Mineralogist*, vol. 41, no. 3, pp. 727–748, 2003.

[57] R. F. Martin and C. De Vito, "The late-stage miniflood of Ca in granitic pegmatites: an open-system acid-reflux model involving plagioclase in the exocontact," *Canadian Mineralogist*, vol. 52, no. 2, pp. 165–181, 2014.

[58] A. Pieczka, A. Szuszkiewicz, E. Szełęg, and K. Nejbert, "Calcium minerals and late-stage Ca-metasomatism in the Julianna pegmatitic system Góry Sowie Block, SW Poland," *Canadian Mineralogist*, vol. 57, no. 5, pp. 775–777, 2019.

[59] J. M. Pyle and F. S. Spear, "Yttrium zoning in garnet: coupling of major and accessory phases during metamorphic reactions," *American Mineralogist*, vol. 88, no. 4, pp. 708–708, 2003.

[60] R. Thomas, J. D. Webster, D. Rhede et al., "The transition from peraluminous to peralkaline granitic melts: evidence from melt inclusions and accessory minerals," *Lithos*, vol. 91, no. 1–4, pp. 137–149, 2006.

[61] A. Müller, J. Spratt, R. Thomas, B. J. Williamson, and R. Seltmann, "Alkali-F-rich albite zones in evolved NYF pegmatites: the product of melt-melt immiscibility," *Canadian Mineralogist*, vol. 56, no. 4, pp. 657–687, 2018.

[62] I. Kobayashi, *Geological map of Kinkasan*, Geological Survey of Japan, 1974.